Global Linear Parameter-Varying Modeling of Flapping-Wing Dynamics Using Flight Data

Armanini, Sophie; Karasek, Matej; de Visser, Coen

DOI
10.2514/1.G003505

Publication date
2018

Document Version
Accepted author manuscript

Published in
Journal of Guidance, Control, and Dynamics: devoted to the technology of dynamics and control

Citation (APA)
Armanini, S., Karasek, M., & de Visser, C. (2018). Global Linear Parameter-Varying Modeling of Flapping-Wing Dynamics Using Flight Data. *Journal of Guidance, Control, and Dynamics: devoted to the technology of dynamics and control*, *41*(11), 2338-2360. https://doi.org/10.2514/1.G003505

Global linear parameter-varying modelling of flapping-wing dynamics using flight data

S. F. Armanini [*], M. Karásek [†], and C. C. de Visser [‡]

Delft University of Technology, Delft, 2629HS, The Netherlands

Taking full advantage of the favourable flight properties of biologically-inspired flapping-wing micro aerial vehicles requires having insight into their dynamics and providing adequate control in all flight conditions. Due the high complexity of flapping flight and limited availability of accurate flight data, however, global models are not readily available, particularly models validated with flight data and suitable for practical applications. This paper proposes an approach for global modelling of nonlinear flapping-wing dynamics, constructing a linear parameter-varying model from a set of local linear models. The model parameters and scheduling functions are determined using system identification, from free-flight data collected on a real test platform over a significant part of the flight envelope. The resulting model allows for the dominant parts of the dynamics to be accurately represented across the considered range of conditions. With 25 parameters overall, it significantly improves on the starting point of 46 local models with 12 parameters each. Moreover, a single model that adapts to the flight condition provides flexibility and continuous coverage, highly useful for simulation and control applications. While in the explored part of the flight envelope nonlinearity was found to be limited, the approach is scalable and expected to also cover larger variations.

[*]PhD Student, Control and Simulation Section, Faculty of Aerospace Engineering, Delft University of Technology; Kluyverweg 1, 2629HS, Delft, The Netherlands, Student Member AIAA

[†]Postdoctoral Researcher, Control and Simulation Section, Faculty of Aerospace Engineering, Delft University of Technology; Kluyverweg 1, 2629HS, Delft, The Netherlands

[‡]Assistant Professor, Control and Simulation Section, Faculty of Aerospace Engineering, Delft University of Technology; Kluyverweg 1, 2629HS, Delft, The Netherlands, Member AIAA

I. Introduction

Flapping-wing micro aerial vehicles (FWMAVs) are attracting an ever-increasing interest from the aerospace community. Inspired by natural flyers, they can achieve outstanding manoeuvrability and efficiency at very small scales and low flight velocities. Thanks to their unique properties, FWMAVs are expected to fill in the gap between fixed-wing and rotating-wing vehicles, allowing for unprecedented performance, particularly for flight in complex cluttered environments. Despite significant progress in understanding flapping-wing flight [1, 2, 3, 4], however, FWMAVs remain challenging to model, due to their unsteady aerodynamics and complex time-varying dynamics.

One particular challenge is to obtain models covering different flight conditions. Particularly low-order models of flapping-wing (aero)dynamics typically have a limited applicability range or have not been validated in different conditions with free-flight data [5, 6, 7, 8, 9, 10, 11, 12]. However, it is essential to know how a system behaves in all its operating conditions to ensure an effective performance. Moreover, global models are valuable, if not indispensable, to provide realistic simulation possibilities, support the development of new controllers and allow for more advanced control approaches. A limited validity domain is particularly constraining for FWMAVs, which can often operate in very different flight regimes. In the context of control and simulation, an added challenge is that models must be not only accurate, but also computationally efficient and suitable for practical use. Hence, simplified models are preferable when they achieve sufficient accuracy. When flight data are available, an alternative to complex and computationally expensive numerical or first-principles models is therefore system identification. This approach is not yet widespread due to the difficulty of obtaining suitable data, however existing work [5, 13, 14, 15, 6, 7, 16] shows it can yield models that are realistic, relatively simple and applicable for control.

This paper addresses the challenge of global data-driven modelling of flapping-wing vehicles, using the example of an existing FWMAV. Starting from free-flight data, we identified a model of the time-averaged longitudinal vehicle dynamics that covers a significant part of the flight envelope for the current vehicle configuration. Based on preliminary data analysis and local modelling results, the global dynamics were approximated using a linear parameter-varying (LPV) modelling approach, starting from a set of local linear time-invariant (LTI) models. LPV modelling is based

on the idea that a global model can be obtained by interpolating between (often linear) local models [17, 18, 19]. While many effective global model identification approaches have been suggested in the aerospace literature [20, 21, 22], the LPV approach is attractive due to its simplicity, in terms of flight testing, modelling and implementation, avoiding high-order model structures and global identification experiments. LPV control and modelling have been applied to a variety of dynamic systems, including aircraft [23, 24, 25, 26, 27, 28, 29, 30], but not yet FWMAVs. Hence, while the aim of this study was to develop an accurate low-order global model for a specific FWMAV, it also generally investigated the applicability of an LPV approach to model flapping-wing dynamics.

Given that no first principles model of the test platform was available, we opted for an identification approach, involving two steps: firstly, local linear models were identified from free-flight data collected on the vehicle; secondly, a set of interpolating functions were determined to combine these models into a global LPV model. Potential scheduling variables were selected based on analysis of the flight data and of the local models, while the scheduling functions defining the LPV model were determined using stepwise regression [31]. The resulting global model was evaluated through comparison with both flight data and local models. To evaluate the robustness and reliability of the results, evaluations were also performed using validation data.

This paper is organised as follows. Section II describes the test vehicle and flight data used. Section III introduces the local models at the basis of the global modelling approach and briefly evaluates these models and the flight data, focusing on the observations relevant for global modelling. Section IV outlines the LPV modelling approach used to transition from the local models to the global model. Section V presents the final model structure and results, and evaluates the obtained LPV model in comparison to flight data. Section VI summarises the main conclusions.

II. Methods and experimental data

A. Test vehicle

The subject of this study was a four-winged FWMAV [32] (cf. Fig. 1) with a 280mm wing span, flapping frequencies of 10-15Hz and a flight envelope ranging from near hover to fast forward flight. While speeds up to 7m/s were previously achieved on this FWMAV by shifting its centre

of gravity (CG) through physically moving parts of the payload (e.g. battery, wings), the speeds achievable in the standard configuration range from approximately near hover to 1.5m/s. The mylar foil wings have an 'X'-configuration, allowing for increased lift production thanks to the clap-and-peel effect. The T-shaped styrofoam tail provides static stability and separates most of the manoeuvring from the wing flapping, such that conventional fixed-wing control mechanisms can be used. This type of vehicle has been the subject of extensive previous research and details of the design can be found in Ref. [32]. The mass and inertia properties of the specific FWMAV used in this study are given in Table 1. Fig. 1b shows the body-fixed coordinate frame used in this study, centred at the vehicle's CG. Contrary to convention, the z-axis was defined to be aligned with the fuselage, to avoid singularities due to the large typical pitch attitude of this FWMAV (cf. Fig. 3a), while avoiding the lack of physical interpretability of quaternions. The forces and moments were defined accordingly (X force aligned with x_B axis, M moment around y_B axis, etc.), with signs following a right-hand convention. Note that a nose-down pitch rate is thus positive.

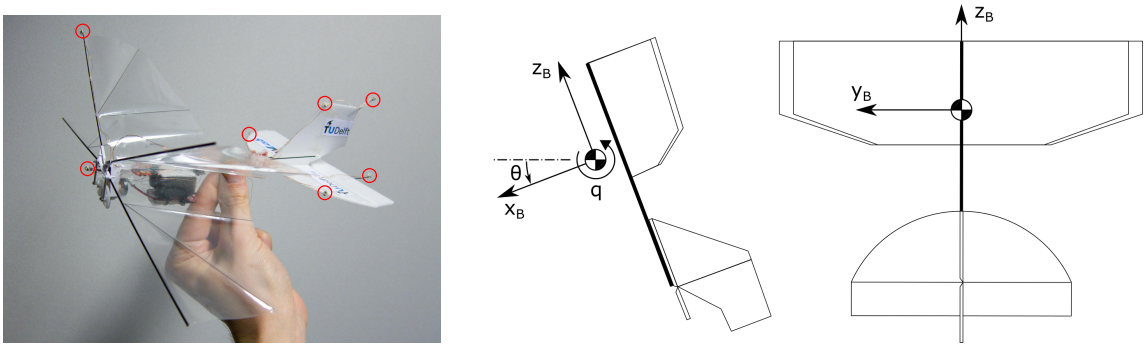

a) Test platform (DelFly II [33]); LED markers used for tracking circled

b) Body-fixed coordinate frame, centred at the CG

Figure 1: Test platform used in this study and body-fixed coordinate system x_B, y_B, z_B

Table 1: Mass and inertia properties of the test platform.

Property	**Value**
$m[kg]$	0.0235
$x_{CG}[m]$ (below fuselage)	0.0096
$y_{CG}[m]$	0
$z_{CG}[m]$ (from wing leading edge)	- 0.0695
$I_{xx}, I_{yy}, I_{zz}[Nm^2]$	7.5×10^{-5}, 6.6×10^{-5}, 1.9×10^{-5}
$I_{xy}, I_{yz}, I_{xz}[Nm^2]$	0, 0, 8.5×10^{-6}

B. Flight data acquisition

The modelling discussed in this paper was based on a set of flight data collected on the test vehicle. The data were collected using a motion tracking system (24 OptiTrack Flex13 cameras, covering a 10m×10m×7m volume) in combination with an on-board inertial measurement unit (IMU) attached to the vehicle. The tracking system was used to measure the positions of seven active LED markers attached to the vehicle at the positions shown in Fig. 1a, allowing for the reconstruction of body position and orientation, control surface deflections and wing leading edge movement, all at 120Hz. The 6-axis IMU, incorporated in the vehicle's Lisa/S autopilot, was used to measure linear accelerations and angular velocities at 512Hz. A sensor fusion approach based on extended Kalman filtering was applied to combine the different measurements, leading to accurate high-resolution measurements [34]. The flight tests involved elevator doublets (cf. Sec. III), executed by the autopilot when triggered by the pilot [35]. A detailed discussion of the hardware, test setup and data processing can be found in Refs. [36] and [35], which describe earlier flight tests conducted on the same type of FWMAV.

C. Flight test data

In line with aerospace convention, the flight envelope was defined in terms of combinations of the angle of attack (AOA) and velocity. Additionally, the flapping frequency was initially considered as a third variable influencing the flight regime. Flight test conditions were selected on the basis of previous tests on the same platform [35, 37], and covered trim velocities ranging approximately from 0.5 to 1.3m/s, AOAs from 40 to 80°, and flapping frequencies from 10 to 14Hz (cf. Fig. 2). While in absolute terms this range is small, considering the small scale of the vehicle the range is significant and in fact represents almost the entire flight envelope achievable with the current vehicle configuration. CG shifts can be used to further enlarge the flight envelope (cf. Sec. A), however, due to the restricted test flight space and because the current study constitutes an investigation into the modelling methodology, no CG shifts were considered. Moreover, flight testing revealed noticeable changes in flight behaviour already within the aforementioned range.

46 short (2-5s) manoeuvres for system identification were recorded. Due to the manual trim-

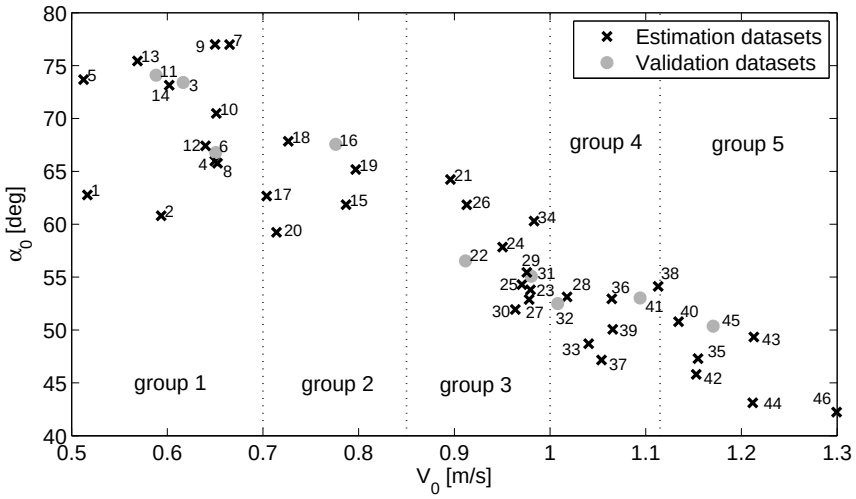

Figure 2: Trim conditions for each of the 46 datasets analysed ($V_0 := ||V||_0$; validation sets as grey circles).

ming procedure and inevitable slight differences between separate flights, the exact same flight condition could not be replicated repeatedly. Rather, a grid of trim conditions was covered, cf. Fig. 2. The test manoeuvres were subdivided into five similarly sized groups (cf. Fig. 2) to facilitate the selection of suitably distributed validation sets. It can be seen in the figure that the data do not uniformly cover the potentially achievable rectangular domain given by the upper and lower bounds of the velocity and AOA. Instead, a limited area around a two-dimensional line is covered. This does not point to incompleteness of the data, rather, it suggests that there is some correlation between velocity and AOA, and that the inherently stable FWMAV is pulled towards an equilibrium condition. The typical operating conditions of the vehicle thus fall within this range. The coverage within the range considered is also not even: in particular, there is a sparser region in the middle. Finally, it should be noted that the choice of variables to define the flight envelope is to some extent arbitrary, however the chosen selection was found to be effective.

III. Flight envelope analysis and local modelling

Two steps were performed prior to developing global models, to glean information on the system and select a global modelling approach. Firstly, the collected flight data were evaluated, and, secondly, local linear models were identified. Both evaluations focused on the time-averaged behaviour, under the assumption that the flapping component can be neglected due to time-scale

separation, found to be acceptable for system-level dynamic analysis of this entomopter [16]. This assumption was also introduced to simplify the evaluation of the global modelling approach. For analogous reasons, only the longitudinal dynamics were considered. This section discusses the findings of the aforementioned preliminary evaluations. The local models also constitute the basis of the global modelling process developed subsequently in this paper.

A. Local model estimation

While flapping-wing dynamics are highly complex, warranting investigation into multi-body modelling [38, 9, 39, 40], several studies have demonstrated that for basic considerations, e.g. in the context of design and control work, the conventional fixed-wing aircraft equations of motion represent a suitable description for many insects and FWMAVs [4, 41, 42, 16]. Thus, local models were obtained using a simplified approach, shown in previous work to yield accurate local models for the studied test platform [16]. The time-averaged longitudinal dynamics were assumed to have the following linear time-invariant (LTI) structure [16]:

$$\begin{bmatrix} \Delta\dot{q} \\ \Delta\dot{u} \\ \Delta\dot{w} \\ \Delta\dot{\Theta} \end{bmatrix} = \begin{bmatrix} \frac{M_q}{I_{yy}} & \frac{M_u}{I_{yy}} & \frac{M_w}{I_{yy}} & 0 \\ \frac{X_q}{m} - w_0 & \frac{X_u}{m} & \frac{X_w}{m} & g\cos(\Theta_0) \\ \frac{Z_q}{m} + u_0 & \frac{Z_u}{m} & \frac{Z_w}{m} & g\sin(\Theta_0) \\ 1 & 0 & 0 & 0 \end{bmatrix} \begin{bmatrix} \Delta q \\ \Delta u \\ \Delta w \\ \Delta\Theta \end{bmatrix} + \begin{bmatrix} \frac{M_{\delta_e}}{I_{yy}} \\ \frac{X_{\delta_e}}{m} \\ \frac{Z_{\delta_e}}{m} \\ 0 \end{bmatrix} \Delta\delta_e \tag{1}$$

The above model structure is based on the nonlinear fixed-wing aircraft equations of motion, with minor differences in the linearisation process (e.g. accounting for the large pitch attitude in flight). An LTI model of the dynamics was identified from each of the 46 flight manoeuvres (cf. Sec. C), resulting in 46 local models. In each manoeuvre, elevator doublets were used to excite the system, having been found, in previous work, to provide suitable excitation, and generally to be an effective compromise given the limited testing space and the linear modelling approach [37, 35] (for turther discussion of the input design see [35, 43]). From each dataset, the parameters (stability and control derivatives) in Eq. 1 were determined using a maximum likelihood estimator, as described in Ref. [16]. Details on the local modelling process can be found in Refs. [16, 35].

With the exception of one case (test # 9), where the estimation data were somewhat unsteady prior to the manouevre and adversely affected the result, the identified local models were found

to be accurate for the corresponding conditions. Table 2 shows the average RMSE and output correlation over all flight tests, for each state. As seen in the table – and discussed in Ref. [16] in the context of similar local modelling work – the accuracy is slightly lower for the velocities, especially w, for which the data appeared to be less informative. By contrast, the pitch dynamics are captured accurately, possibly because they are more affected by the elevator inputs used.

In an attempt to better excite the velocity dynamics, throttle signals (causing changes in flapping frequency) were also initially tested, however they did not yield a significant improvement. It is possible that the velocity dynamics do not vary as significantly as the pitch dynamics, or cannot be excited independently, or would require longer tests (hence a different setup) to be captured. For the purposes of this study, elevator doublets were deemed to provide a sufficient level of accuray, therefore more complex inputs, e.g. based on optimal input design [44, 45], were not considered.

Table 2: Metrics quantifying performance of local models (Eq. 1) (avg.±std. dev. over all flight datasets).

Variable	Output corr.	RMSE(% of meas. range)
q	0.96 ± 0.10	4.2 ± 3.0
u	0.94 ± 0.10	6.2 ± 3.9
w	0.93 ± 0.15	6.8 ± 5.3
Θ	0.97 ± 0.06	3.9 ± 2.6

B. Data and local model analysis

The flight data were analysed to establish how and to what extent the system dynamics change in different flight conditions and hereby to guide the modelling approach. Fig. 4a shows the average flight-measured responses to the same input signal obtained in different ranges of flight conditions (for better readability, the data are divided into three groups in these plots). It can be seen that different trim conditions lead to visible differences in the system response – in both magnitude and especially phase. Moreover, these differences are small – they are likely to be significant, given the overall small scale of the modelling problem, however they are also difficult to model accurately with real, noisy flight data. From flying experience with the studied FWMAV, there were known to be noticeable differences in flight behaviour within the range of conditions considered. However, one additional goal of this study was to evaluate whether a global model is necessary in this range,

a) Time lapse of example identification manoeuvre (time step≈0.27s)

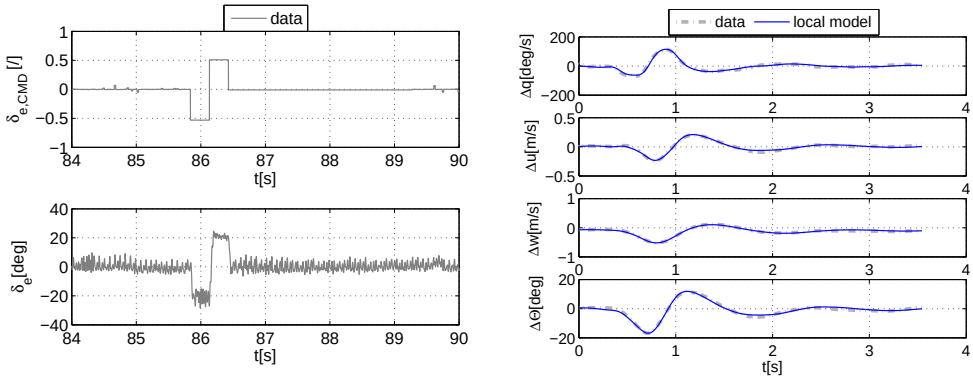

b) Example of identification manoeuvre (measured flight data)

c) Example of local model match with flight data

Figure 3: Local model identification input manoeuvre and results example.

and whether such small-scale differences can be modelled using real-world data.

Next, the obtained local models were considered. As observed in previous work [37, 16], the longitudinal dynamics of the FWMAV (Fig. 4b) are characterised by one oscillatory pole and two aperiodic poles, all of which are stable, except in two of the identified local models, which have an unstable real pole. These two models are most likely unstable due to the more noisy/unsteady identification data they were determined from. In view of our limited knowledge of the vehicle dynamics, interpreting the identified models is not straightforward, however the types of eigenvalues found are in agreement with most results in the flapping-wing literature [4, 41, 42, 11] (though in insects the oscillatory mode is unstable). The oscillatory mode seems comparable to a short period mode (with the most dominant state being the pitch rate), while, as for other flapping-wing flyers, no phugoid appears to exist. While the faster aperiodic mode varies somewhat between datasets and is not easy to interpret, it is interesting to note that the slower aperiodic pole, identified

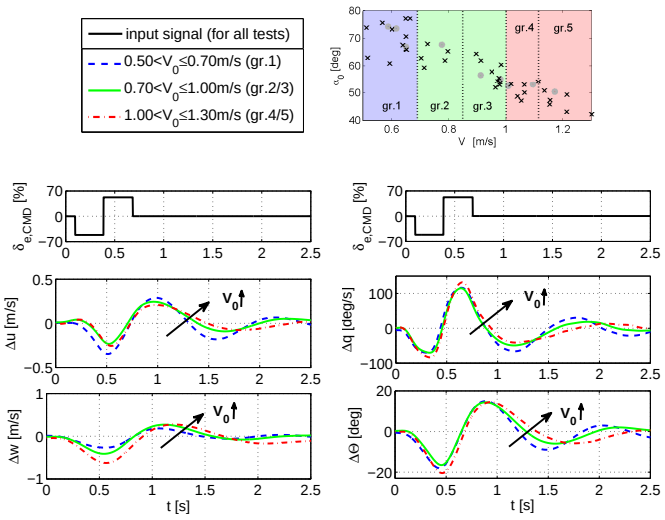

a) Average responses in different flight envelope regions.

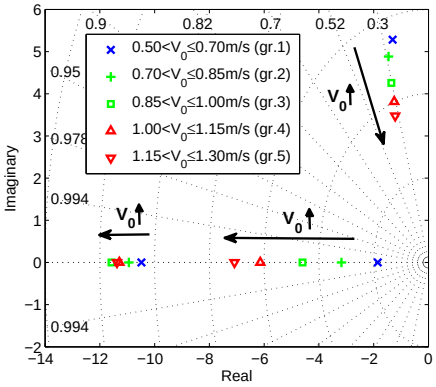

b) Local model poles: average in different flight envelope regions.

Figure 4: System dynamics and output versus flight condition (average for groups of datasets, cf. Fig. 2)

more consistently, involves all states to a fairly significant extent (average normalised eigenvector $|v_4| = [0.42, 0.28, 0.16, 0.11]^T$).

As anticipated from the flight data analysis, several trends were found in the system dynamics. With increasing velocity and decreasing AOA, the oscillatory pole pair moves towards lower frequencies, while the damping varies only to a minor extent and less clearly. The slower aperiodic pole moves from approximately -1 to -10 (considering all datasets) with increasing velocities, indicating an increase in stability. The faster pole, by contrast, varies less and less consistently – the latter may be due to insufficiently informative data, as discussed previously. It was indeed found that some of the parameters connected to the w-velocity were estimated less effectively, resulting in higher variances (cf. Sec. D), which in turn may have affected this particular eigenmode. Some trends were also observed in the control behaviour, with the vehicle becoming more responsive to elevator deflections at higher velocities. As expected, this is mainly evident in the pitch rate response to the elevator, whilst the (indirect) effect on the velocities is both less significant overall and less affected by the flight condition (cf. Sec. D).

The system dynamics are discussed and shown in more detail in Sec. C, after the final model structure has been established. However, the initial evaluation in this section already shows that the dynamics vary within the operating domain considered, motivating the need for global modelling.

C. Main conclusions for global modelling

From the analysis in the previous sections, two main conclusions were drawn that are relevant for global modelling. Firstly, it was found that LTI models of the suggested form (Eq. 1) achieve a high accuracy at the local level and can represent the system dynamics in the entire flight envelope region analysed. This implies that the simplest approach for global coverage is to somehow combine the available local models – an approach that is also advantageous from a control perspective, as many established control methods are available for LTI systems. Secondly, within this region, there is a correlation between the local system dynamics and the flight conditions the respective local models refer to. These two points suggest that linear models provide a suitable local description, but also that the flight dynamics are in fact nonlinear, at least to some extent, and hence that global modelling is relevant. Based on these observations, a linear-parameter-varying (LPV) approach was deemed a suitable and indeed advantageous way to model the observed nonlinearity.

The preceding analysis also raised a number of questions to be considered in the global modelling process. As discussed, one challenge identified was the fact that the observed differences between local models are, in an absolute sense, small. They may still have a considerable impact, given the "micro" problem scale, but are also challenging to model using noisy flight data. Another challenge found was the fact that some components of the local dynamics could not be identified as reliably as the rest, possibly due to insufficient excitation (cf. also Sec. D). While the aforementioned factors complicate the global modelling process, the overall accuracy of the local models was nonetheless high. Furthermore it is possible for a global model to improve on local results, by ignoring single outlier results in favour of overall trends. To improve the final result as far as possible and address the issue of unreliably-estimated components without recurring to additional flight tests (which are always constrained by the available flight test setup, cf. Sec. A), the local model structure was re-assessed prior to the global modelling, as discussed in the next section.

D. Simplified local model

Given that the LPV model was constructed from the local models, an important preliminary step was to ensure that the local results were as accurate and reliable as possible. While overall the

local models were accurate, the local model structure was therefore revisited, to determine whether the separate local model parameters were well-estimated and whether they were all necessary in the model structure. Parameters that have no significant effect on the dynamics are estimated inaccurately and can adversely influence the modelling results if kept in the model structure.

First, the estimated model parameters themselves were considered, i.e. how they were distributed and how much and in what way they varied. Some variation was expected, due to the different flight conditions covered, however if the estimates for the same local parameter obtained from different datasets vary erratically or to an implausible extent, the parameter is likely not estimated reliably. It can for instance be observed in Fig. 5 that X_w and Z_{δ_e} vary significantly between different local models, in both magnitude and sign. Given that the final state-output predicted by the local models was nonetheless accurate for all datasets, the significant variation suggests that these parameters have no significant effect on the overall model and can be discarded from the local model structure. To a lesser extent, similar observations were made for all Z-related parameters.

To evaluate the identifiability of single local model parameters, the estimated covariance matrices (Cramér-Rao bounds) of the local models were considered next. Fig. 6 shows the estimated standard errors ($\hat{\sigma} := +\sqrt{var(\hat{\theta})}$) of the model parameters, specifically the distribution of the errors obtained for all local models. It can be observed that for some of the parameters, particularly those related to the Z-force and/or the w velocity, the standard errors tend to be higher, with values frequently above 10% and reaching up to 50% in some cases. This implies that a lower confidence can be placed on the estimated parameter values, which points to a lower identifiability and partially explains the seemingly more random variation of said parameters with the flight condition. For the remaining parameters, standard errors are mostly low for all datasets, typically below 5% and often much lower – suggesting that the local values are reliable.

Finally, the estimated correlation coefficient between pairs of parameters in the local models was considered. While the correlations between parameter pairs rarely exceed the critical value of 0.9 [31], the values obtained provide insight into which parameters have similar effects. The w velocity-related parameters were found to be generally more correlated to other parameters. With one exception, the correlations between parameters were only found to exceed the critical

value in isolated cases, all of these occurring in the same two local models, which presumably were not effectively estimated as a whole. The exception is the parameter pair $[Z_q, Z_{\delta_e}]$: these two parameters were found to be almost fully correlated (corr>0.98) in many of the local models, suggesting that for one of the reasons mentioned in Sec. B they cannot be estimated separately with reliability, and hence it is advisable to drop one of the two from the model structure.

Based on the preceding evaluation, the less reliably estimated local parameters were fixed to zero a priori, i.e. excluded from the model structure, so that the main effects could be better captured by the remaining parameters, in turn facilitating the construction of an accurate global model and improving the results. Specifically, the following parameters were discarded: X_w, Z_u, Z_{δ_e}. The decision to discard Z_u rather than Z_w was to some extent arbitrary, as both parameters appeared to be unreliable to a similar extent. Z_q was retained because it was found to affect the result, despite not being estimated very accurately. The following simplified model structure resulted:

$$\begin{bmatrix} \Delta\dot{q} \\ \Delta\dot{u} \\ \Delta\dot{w} \\ \Delta\dot{\Theta} \end{bmatrix} = \begin{bmatrix} \frac{M_q}{I_{yy}} & \frac{M_u}{I_{yy}} & \frac{M_w}{I_{yy}} & 0 \\ \frac{X_q}{m} - w_0 & \frac{X_u}{m} & 0 & g\cos(\Theta_0) \\ \frac{Z_q}{m} + u_0 & 0 & \frac{Z_w}{m} & g\sin(\Theta_0) \\ 1 & 0 & 0 & 0 \end{bmatrix} \begin{bmatrix} \Delta q \\ \Delta u \\ \Delta w \\ \Delta\Theta \end{bmatrix} + \begin{bmatrix} \frac{M_{\delta_e}}{I_{yy}} \\ \frac{X_{\delta_e}}{m} \\ 0 \\ 0 \end{bmatrix} \Delta\delta_e \tag{2}$$

Results were slightly better than for the original model, in terms of output accuracy (cf. Table 3), consistency and reliability, while requiring fewer parameters. While the Z-equation parameters were still less accurately estimated than the rest, the parameter covariances improved (cf. Fig. 7) even for these parameters. The remaining parameters were estimated reliably (cf. also Sec. B), and highly correlated parameters no longer occurred. The parameter trends given by the new model structure are shown in Figs. 10-11, in the discussion of the scheduling results.

IV. Global modelling

A. LPV approach

Linear parameter-varying (LPV) modelling is related to the idea of gain scheduling in control [46, 47]. The underlying concept is that at every point in the operating domain of a system a linearised model can be obtained, and that a function can be found to interpolate between these

linearised models, based on one or more scheduling variables. As a result, the same model structure can be used to describe the entire operating domain, in dependence on a set of scheduling variables. Ideally, the scheduling variables should be exogenous and independent of the system dynamics [48, 49]. Hence, LPV methods are best suited to systems with clearly defined, discrete operating conditions, where independent external scheduling variables can be easily defined. Nonetheless, the LPV approach has been applied to systems that do not strictly meet this requirement, including aircraft [23, 24, 25]. Many aircraft applications in fact use a quasi-LPV approach (sometimes also called stitching [30]), where the scheduling variables are (or depend on) system states but are assumed to be independent. Furthermore, many aerospace examples of LPV modelling linearise an available nonlinear model to obtain a linearised model structure that contains the chosen scheduling variables [24, 29]. The aim is frequently to simplify the nonlinear model to allow for simpler control approaches to be applied.

In the current study, no baseline model was available, thus it was not possible to derive from first principles an LPV model structure, where the scheduling variables could be defined intuitively and related to physical parameters. Instead, the choice of scheduling variables functions was to some degree arbitrary. The LPV model was implemented by scheduling the individual model parameters, i.e. the state-space matrices in Eq. 1, as described in Sec. B. Note that while the term scheduling is adopted to describe the functions used to approximate the changes between local models, the resulting global model is not identical to the local models at the flight conditions the latter are estimated in. In fact, given that the baseline local models are themselves not ideal, *true* descriptions of the system, and that the observed variation in local dynamics may not depend exclusively on the chosen scheduling variables, it was considered inadvisable to interpolate between the local models. Doing so would have resulted in highly complex functions, both counteracting the object of simplified modelling, and almost inevitably producing a global model that captures the error as well as the system dynamics. Instead, it was considered preferable to find a function that approximates the most significant trends observed in a somehow optimal way. The chosen approach was based on the assumption that the parameters are sufficiently uncorrelated to each other (cf. also Sec. D) and that the model structure remains the same for all conditions considered.

Both assumptions were already made, implicitly, in the local modelling process, and, while both are not wholly valid, the local results suggests that they are acceptable.

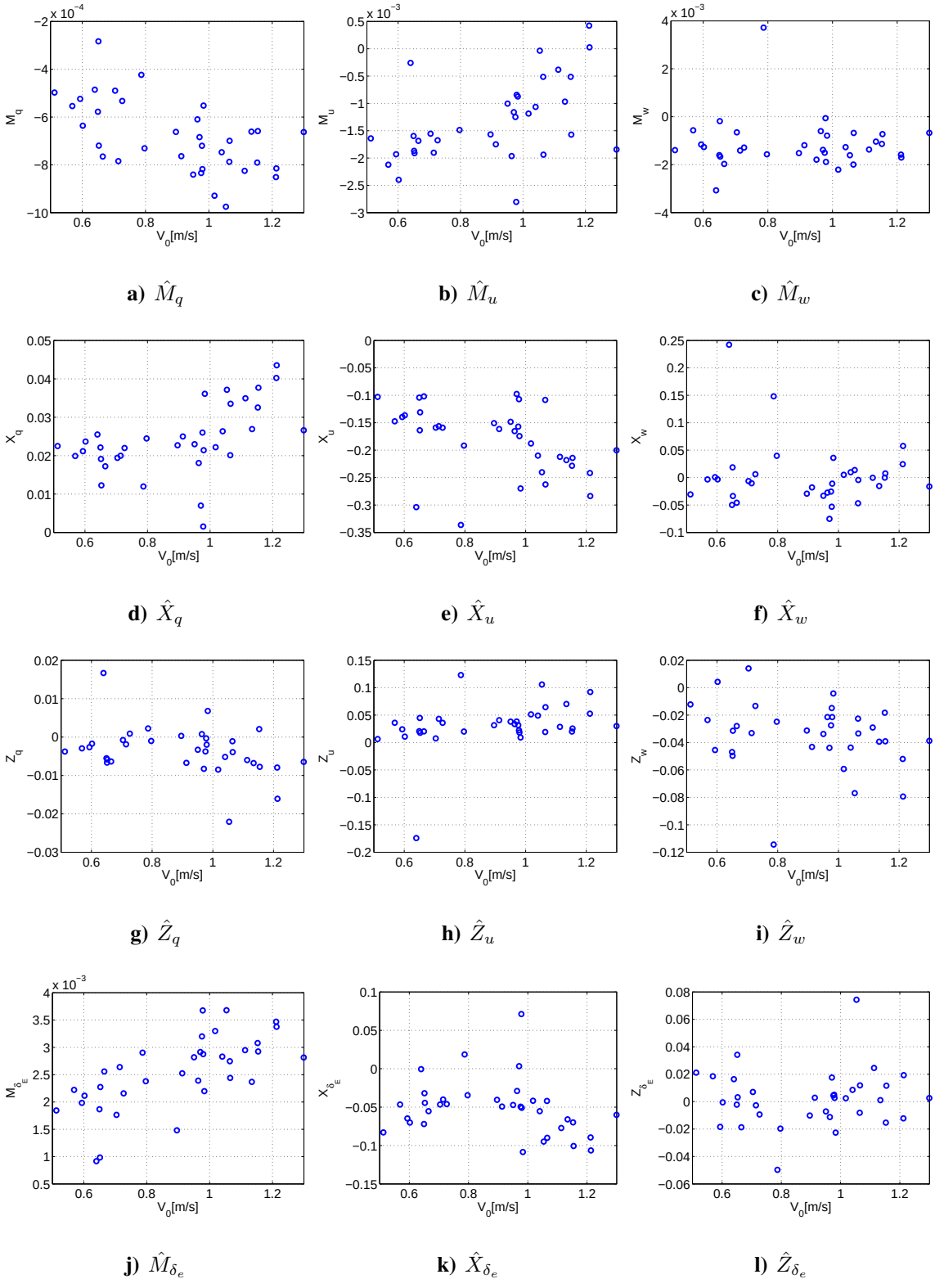

a) $\hat{M}_q$ **b)** $\hat{M}_u$ **c)** $\hat{M}_w$

d) $\hat{X}_q$ **e)** $\hat{X}_u$ **f)** $\hat{X}_w$

g) $\hat{Z}_q$ **h)** $\hat{Z}_u$ **i)** $\hat{Z}_w$

j) $\hat{M}_{\delta_e}$ **k)** $\hat{X}_{\delta_e}$ **l)** $\hat{Z}_{\delta_e}$

Figure 5: Local LTI model parameters versus flight velocity (cf. Fig. 2).

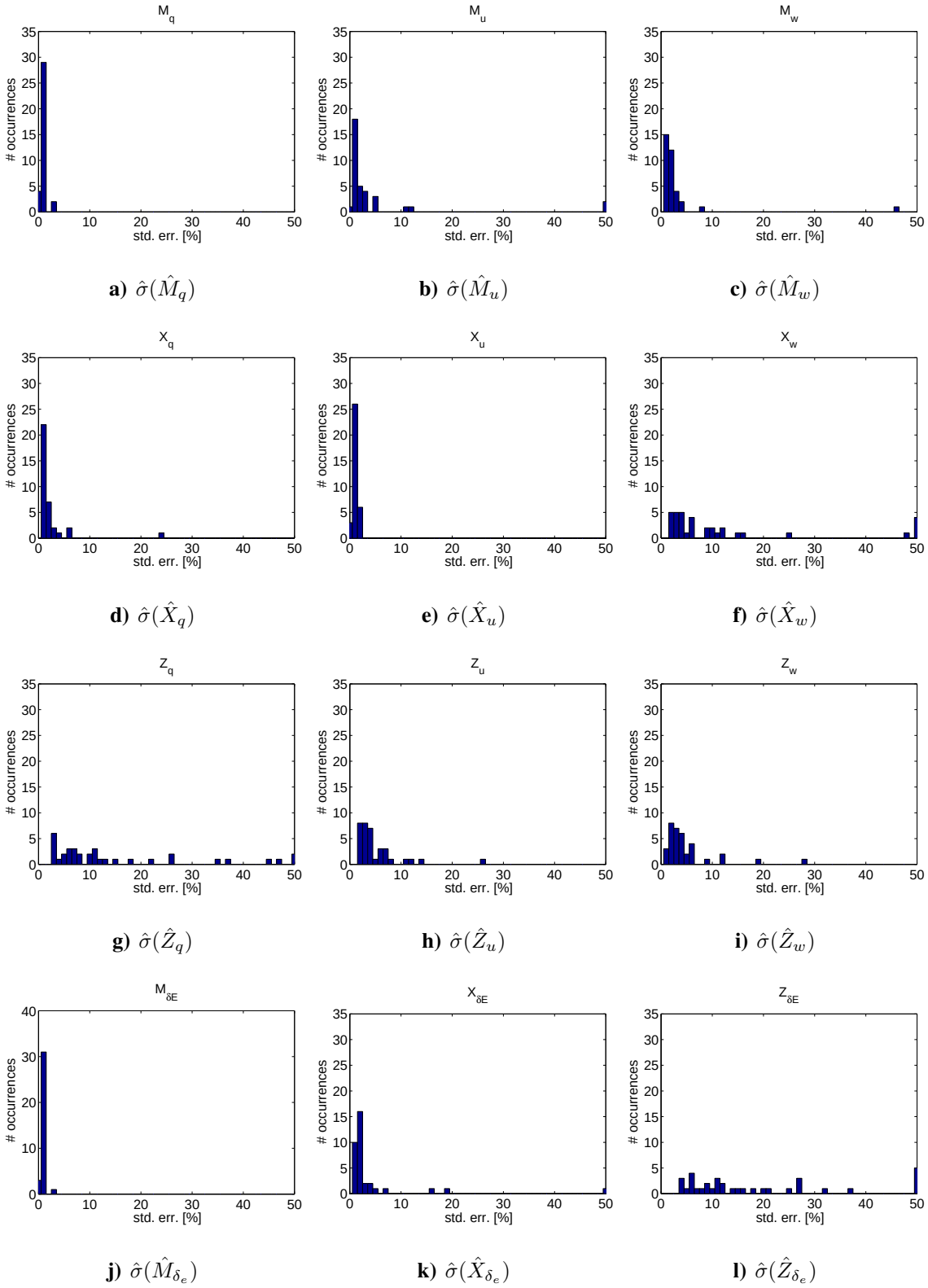

a) $\hat{\sigma}(\hat{M}_q)$ **b)** $\hat{\sigma}(\hat{M}_u)$ **c)** $\hat{\sigma}(\hat{M}_w)$

d) $\hat{\sigma}(\hat{X}_q)$ **e)** $\hat{\sigma}(\hat{X}_u)$ **f)** $\hat{\sigma}(\hat{X}_w)$

g) $\hat{\sigma}(\hat{Z}_q)$ **h)** $\hat{\sigma}(\hat{Z}_u)$ **i)** $\hat{\sigma}(\hat{Z}_w)$

j) $\hat{\sigma}(\hat{M}_{\delta_e})$ **k)** $\hat{\sigma}(\hat{X}_{\delta_e})$ **l)** $\hat{\sigma}(\hat{Z}_{\delta_e})$

Figure 6: Estimated standard errors for each local LTI parameter estimate, using the **full model structure (Eq. 1).**

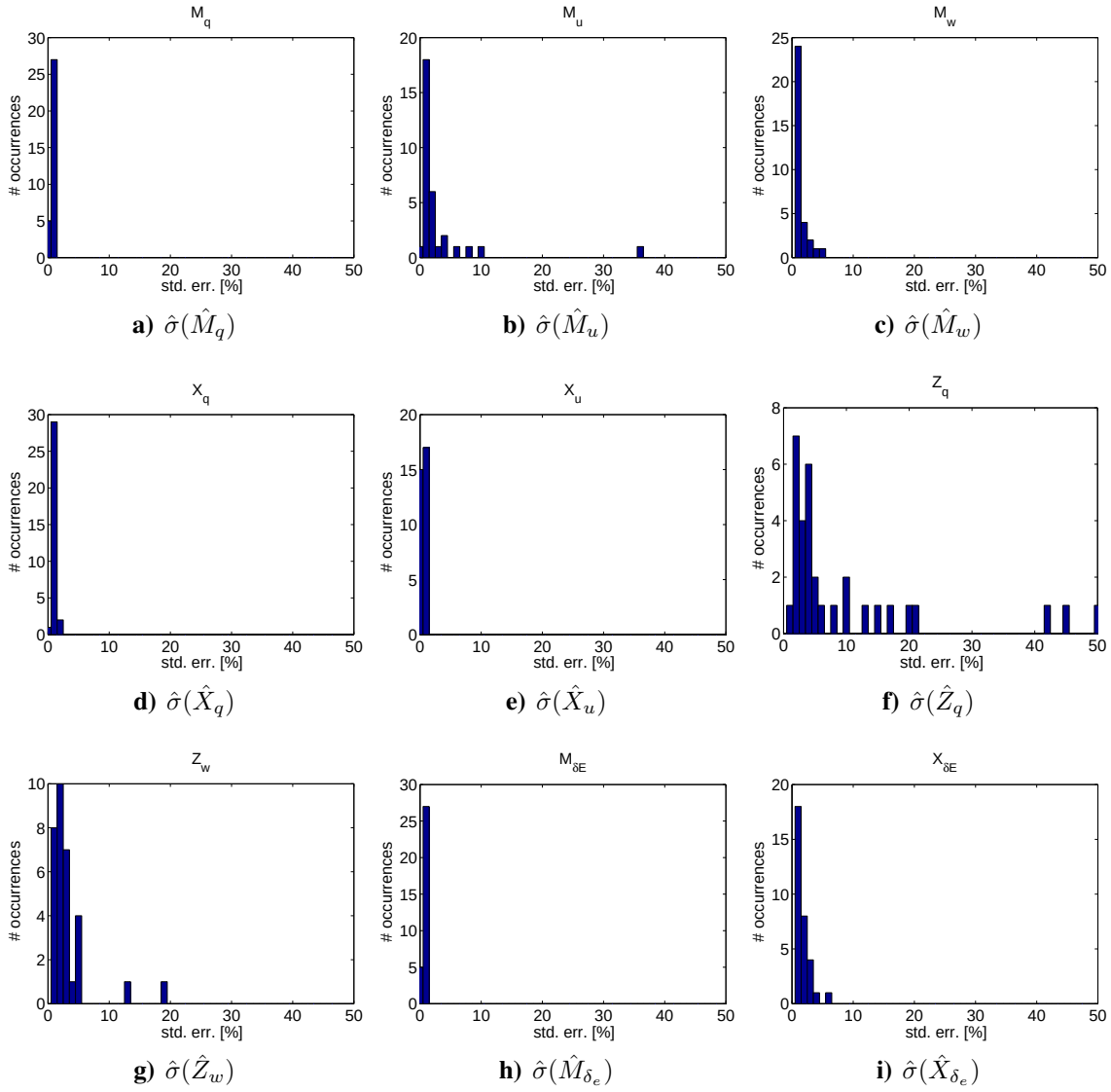

a) $\hat{\sigma}(\hat{M}_q)$ **b)** $\hat{\sigma}(\hat{M}_u)$ **c)** $\hat{\sigma}(\hat{M}_w)$

d) $\hat{\sigma}(\hat{X}_q)$ **e)** $\hat{\sigma}(\hat{X}_u)$ **f)** $\hat{\sigma}(\hat{Z}_q)$

g) $\hat{\sigma}(\hat{Z}_w)$ **h)** $\hat{\sigma}(\hat{M}_{\delta_e})$ **i)** $\hat{\sigma}(\hat{X}_{\delta_e})$

Figure 7: Estimated standard errors for each local LTI parameter estimate, using the **simplified model structure** (Eq. 2).

The following sections outline the LPV modelling approach formulated in this study. An in-depth treatment of the general LPV modelling framework can be found in the literature [17, 49, 48].

B. Scheduling formulation

As for the local modelling, the first step in the global model identification process was to define a model structure. For LPV modelling, this involves defining both a local model structure and a set of scheduling functions to combine the local models. In view of the already available local models, the structure of the LPV model was based on that of the local models (cf. Eq. 1), however in the

Table 3: Metrics quantifying performance of simplified local models (Eq. 2); (avg.±std.dev. over all datasets).

Variable	Output corr.	RMSE (% of meas. range)
q	0.97 ± 0.02	4.0 ± 1.2
u	0.96 ± 0.02	5.7 ± 1.9
w	0.94 ± 0.07	6.9 ± 3.2
θ	0.98 ± 0.02	3.9 ± 1.2

LPV model each parameter is a function of some of the states rather than a constant, i.e.:

$$\dot{\mathbf{x}} = \mathbf{A}(\rho)\mathbf{x} + \mathbf{B}(\rho)\mathbf{u} \tag{3}$$

where ρ is the vector of scheduling variables and the system matrices $\mathbf{A}$ and $\mathbf{B}$ depend on ρ. Assuming the dependence on the scheduling variables is affine, this can be written out as:

$$\mathbf{A}(\rho) = \mathbf{A}_0 + \mathbf{A}_1\rho(1) + \mathbf{A}_2\rho(2) + \ldots + \mathbf{A}_n\rho(n) \tag{4}$$
$$\mathbf{B}(\rho) = \mathbf{B}_0 + \mathbf{B}_1\rho(1) + \mathbf{B}_2\rho(2) + \ldots + \mathbf{B}_n\rho(n) \tag{5}$$

where the bracketed number denotes the corresponding component in the scheduling vector ρ, and the matrices $\mathbf{A}_i$ and $\mathbf{B}_i$ are matrices of coefficients for the ith of the n elements in the scheduling vector. The matrices on the right hand side do not have to be full, and in the current problem are mostly sparse (cf. Eq. 16).

Once the underlying local model structure has been defined, the key question in devising an LPV model structure is the selection of suitable scheduling variables. In conventional fixed-wing problems, LPV models are typically scheduled based on either flight states, or configuration-related variables [23, 28, 29, 30]. Based on the analysis in Sec. B and on previous work [37, 35], and given that a single configuration (CG and geometry) was considered, functions of the (trim) angle of attack (AOA), total velocity and flapping frequency were considered as a basis for scheduling in the current model. Given that accurate results were found to be obtainable using only the AOA and velocity, the remainder of this paper focuses on these two variables only. The scheduling variables are thus directly related to the states, and the model formulation can be considered a form of stitching [30]. Moving from the general notation in Eqs. 4–5 to the specific formulation

used in this study, the scheduling vector ρ thus takes the form:

$$\rho_{ij}(V_0, \alpha_0) := V_0^i \alpha_0^j, \quad i \in [0, d], j \in [0, d], \tag{6}$$

where d is the maximum degree considered for each scheduling variable. Note that the full set of possible combinations obtainable from Eq. 6 was merely the starting point for model structure selection: the final model structure includes only a small number of these terms (cf. Sec. C).

Given that certain components of the local model structure are fully determined by kinematic relations, the scheduling was limited to the aerodynamic terms, while the known parts of the local model structure were kept at their known values, or determined from known expressions, as clarified in Eq. 7. In some cases it may be more convenient, in practice, to directly interpolate the entire matrices – in such cases it is straightforward to adjust the current model formulation to also include the kinematic terms, particularly since all of these terms are either constant or known to be related to the chosen scheduling states. The resulting LPV model takes the following form, where tilde superscripts denote parameters estimated from the scheduling functions.

$$\tilde{\mathbf{A}}(V_0, \alpha_0) = \begin{bmatrix} \frac{\tilde{M}_q}{I_{yy}} & \frac{\tilde{M}_u}{I_{yy}} & \frac{\tilde{M}_w}{I_{yy}} & 0 \\ \frac{\tilde{X}_q}{m} - w_0 & \frac{\tilde{X}_u}{m} & \frac{\tilde{X}_w}{m} & g\cos(\Theta_0) \\ \frac{\tilde{Z}_q}{m} + u_0 & \frac{\tilde{Z}_u}{m} & \frac{\tilde{Z}_w}{m} & g\sin(\Theta_0) \\ 1 & 0 & 0 & 0 \end{bmatrix} := \begin{bmatrix} 0 & 0 & 0 & 0 \\ -w_0 & 0 & 0 & g\cos(\Theta_0) \\ u_0 & 0 & 0 & g\sin(\Theta_0) \\ 1 & 0 & 0 & 0 \end{bmatrix} + \sum_{i=0}^{d} \sum_{j=0}^{d} \mathbf{A}_{ij} \rho_{ij}(V_0, \alpha_0) \tag{7}$$

$$\tilde{\mathbf{B}}(V_0, \alpha_0) = \begin{bmatrix} \frac{\tilde{M}_{\delta_e}}{I_{yy}} \\ \frac{\tilde{X}_{\delta_e}}{m} \\ \frac{\tilde{Z}_{\delta_e}}{m} \\ 0 \end{bmatrix} := \sum_{i=0}^{d} \sum_{j=0}^{d} \mathbf{B}_{ij} \rho_{ij}(V_0, \alpha_0) \tag{8}$$

As in Eqs. 4 and 5, $\mathbf{A}_{ij}$ and $\mathbf{B}_{ij}$ are constant matrices of coefficients[a], however, here their subscripts indicate which component of the scheduling vector they refer to. Given that not all permutations given by Eq. 6 were used in the final model structure, and that different parameters were represented by different scheduling functions, several $\mathbf{A}_{ij}$ and $\mathbf{B}_{ij}$ matrices in the above equations are either zero or sparse matrices. As a clarification, the LPV component of Eqs. 7 and 8 can be written out for each parameter in the model structure ($\mathbf{A}$ and $\mathbf{B}$ matrices) as shown below for $\tilde{M}_q$:

[a] $\mathbf{A}_{ij}$ and $\mathbf{B}_{ij}$ contain the *global* model parameters, which are constant for all flight conditions

$$\tilde{M}_q(V_0, \alpha_0) = \sum_{i=0}^{d} \sum_{j=0}^{d} a_{Mq,ij}\rho_{ij} = a_{Mq,00} + a_{Mq,01}\rho_{01} + \ldots + a_{Mq,dd}\rho_{dd} \tag{9}$$

Here $a_{Mq,ij}$ denotes the set of constant global model parameters (contained in the A_{ij} matrices in Eq. 7), which are used to compute $\tilde{M}_q$ at any given flight condition, given the velocity and AOA. Note that in the analogous of the above equation written for parameters in the *local* $\mathbf{B}$ matrix, the *global* model parameters are denoted by a b instead of an a (e.g. $b_{M\delta_e,ij}$). The different notation highlights the relation between the scheduling functions and the local model structure underlying the global model. The derivation of the scheduling functions, and estimation of the global model parameters they contain (A_{ij}, B_{ij}), are explained in the following section.

C. Scheduling function selection and global model parameter estimation

Clearly, Eqs. 4 and 5 result in a large number of terms even if a small polynomial degree d is chosen for the scheduling functions. In fact, only a small number of terms were found to be required on the right hand side of the equations, resulting in a relatively simple final result. To determine which of the potential terms were necessary for an accurate global model, and to determine suitable functions to describe each term in the LPV model, a stepwise regression was implemented, starting from a candidate pool of model terms including all parameters shown in the above equation, up to a degree of $d = 3$ for each model term. The maximum model degree was limited to avoid excessively high orders that might have led to over-fitting. Additionally, lower-order functions are more likely to retain a basic level of physical plausibility.

Given that considering the LPV model output (the model-predicted states) directly in the stepwise regression would have required optimising the model structure for all scheduling functions simultaneously, as well as for all flight conditions simultaneously, resulting in a computationally expensive problem, the problem was simplified by assuming that all local model parameters were entirely uncorrelated (cf. Sec. A). This was considered acceptable based on the low correlations obtained between separate parameters in the local models (cf. Sec. D), and allows for each term in the LPV model to be considered separately. It was thus assumed that finding the optimal model structure for each sub-model would lead to a suitable (albeit not optimal) global model structure.

A stepwise regression was thus conducted for each parameter in the $\mathbf{A}_{ij}$ and $\mathbf{B}_{ij}$ matrices ($\tilde{M}_q, \tilde{M}_u$, etc.), in order to determine a scheduling polynomial to represent the parameter as a function of the scheduling variables (V, α). This was attempted both with the AOA and velocity alone, and with the two aforementioned variables together with the flapping frequency. Initial results demonstrated that a high accuracy could be achieved even if the flapping frequency was excluded – a solution considered preferable as it results in a simpler model structure.

Details on stepwise regression can be found in the literature (e.g., Refs. [50, 31, 51]); a concise overview is given here for completeness. Stepwise regression is a model structure determination process for problems that can be expressed as a linear regression, in the form:

$$\mathbf{z} = \mathbf{X}\boldsymbol{\Theta} + \epsilon \tag{10}$$

where $\boldsymbol{\Theta}$ is a constant parameter vector, ϵ is the equation error, and $\mathbf{z}$ and $\mathbf{X}$ contain the output and regressors, respectively, at each measurement point. Based on the previously stated assumption of uncorrelated local model parameters, each parameter in the local model structure was treated separately. Thus, for each local parameter (M_q, M_u, etc.), the above equation was constructed as follows: the parameter vector contains the global model parameters (e.g. the a terms in Eq. 9) used to represent the *local* model parameter considered; the output vector contains the values the considered local parameter takes in each of the identified local models ($\mathbf{z} \in \mathbb{R}^{n_C \times 1}$, where n_C is the number of flight conditions considered); and the regressor matrix contains functions of V and α computed from measurements at every flight condition, starting from all n_x combinations given by Eq. 6 ($\mathbf{X} \in \mathbb{R}^{n_C \times n_x}$). Each measurement instance (row of $\mathbf{z}$, $\mathbf{X}$ and $\boldsymbol{\epsilon}$) therefore corresponds to a different flight condition. Thus, for instance, for M_q, Eq. 10 takes the form,

$$\begin{bmatrix} M_q(V(1),\alpha(1)) \\ M_q(V(2),\alpha(2)) \\ \vdots \\ M_q(V(n_C),\alpha(n_C)) \end{bmatrix} = \begin{bmatrix} \rho_{00}(1)=1 & \rho_{01}(1)=\alpha(1) & \dots & \rho_{dd}(1)=V^d(1)\alpha^d(1) \\ \rho_{00}(2)=1 & \rho_{01}(2)=\alpha(2) & \dots & \rho_{dd}(2)=V^d(2)\alpha^d(2) \\ \vdots & \vdots & \ddots & \vdots \\ \rho_{00}(n_C)=1 & \rho_{01}(n_C)=\alpha(n_C) & \dots & \rho_{dd}(n_C)=V^d(n_C)\alpha^d(n_C) \end{bmatrix} \begin{bmatrix} a_{Mq,00} \\ a_{Mq,01} \\ \vdots \\ a_{Mq,dd} \end{bmatrix} + \begin{bmatrix} \epsilon(1) \\ \epsilon(2) \\ \vdots \\ \epsilon(n_C) \end{bmatrix} \tag{11}$$

The main limitation of the model formulation in Eq. 10 is that it cannot account for the error in the velocity and AOA measurements, and only considers the error ϵ in the local model parameters, assumed, as per convention, to be white Gaussian noise. Nonetheless, the aforementioned model formulation provides a straightforward means to derive suitable scheduling functions, and was subsequently found to yield accurate final results (cf. Sec. V).

Given an equation of the form of Eq. 10, the goal of the stepwise regression process is to determine which of the n_x regressors in $\mathbf{X}$ need to be retained in order to obtain an accurate model. The stepwise regression thus begins from a pool of candidate regressors, constructed out of permutations of the velocity and AOA, up to the chosen maximum model degree (here, 3; cf. also Eqs. 6 and 9). At each step, the partial correlation of each regressor with the known output z is computed, accounting for any already determined model terms (i.e. we compute the correlation of the regressor to the original output z minus the contribution of the model terms included in previous steps). The regressor x_k leading to the highest partial correlation is considered for inclusion in the model structure, and the (partial) F-statistic is calculated [51] to determine whether the contribution of the selected regressor to the model is significant, i.e. whether F is above a chosen critical value:

$$F_k = \frac{\hat{\theta}_k^2}{\sigma^2(\hat{\theta}_k)} > F_{crit} \tag{12}$$

where $\hat{\theta}_k$ is the considered parameter (which is multiplied by regressor x_k in the model), and σ^2 is the estimated variance of θ_k. If Eq. 12 holds, then the corresponding parameter $\hat{\theta}_k$ is included in the model. Whenever a new model term has been added, the partial F-statistic of all regressors previously included in the model structure must be re-computed, to assess whether their contribution remains significant after the additional variable has been included in the model structure. Any of the previously included regressors whose F-statistic is below the chosen threshold is once again removed from the model. These steps are repeated until some criterion is met: in this study, the change in predicted square error and R^2 coefficient were considered.

After selecting a model structure using the approach described above, the global model parameters were estimated using an ordinary least squares (OLS) estimator, which lends itself well to the model formulation used in the regression. Using the same notation as in Eq. 10, the cost function

to minimise, for each local parameter ('output' $\mathbf{z}$), is given by:

$$\mathbf{J} = \frac{1}{2}\left[\mathbf{z} - \mathbf{X}\boldsymbol{\Theta}\right]^T \left[\mathbf{z} - \mathbf{X}\boldsymbol{\Theta}\right]^T \tag{13}$$

where X^* denotes the final, optimised set of regressors resulting from the stepwise regression. The OLS estimator resulting from the minimisation process is then:

$$\hat{\boldsymbol{\Theta}} = (\mathbf{X}^T\mathbf{X})^{-1}\mathbf{X}^T\mathbf{z} \tag{14}$$

The set of global model parameter vectors $\hat{\boldsymbol{\Theta}}$ (one per local model term) allows for an LTI model to be obtained in any part of the known flight envelope and, theoretically, also to extrapolate beyond this. The latter however requires investigating the boundaries of the flyable envelope and the nonlinearity of the system outside the explored region. The high-level process to determine the scheduling functions and global model parameters is clarified in Fig. 8.

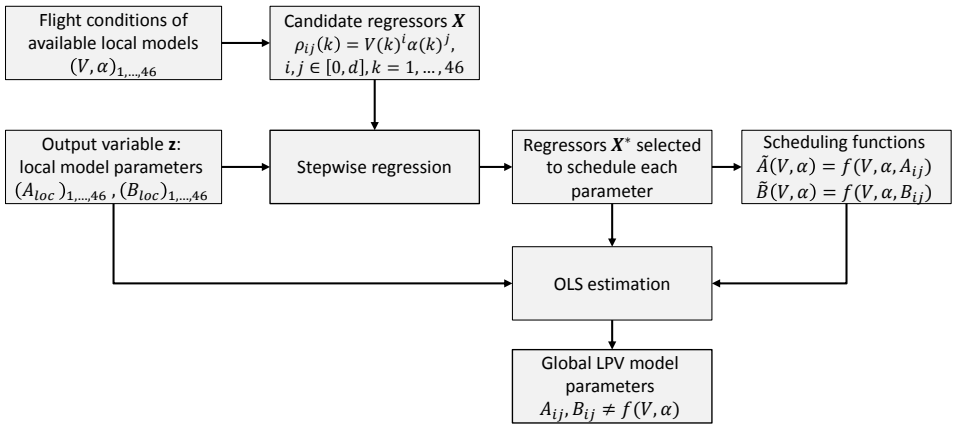

Figure 8: LPV model construction process ($\mathbf{X}^*$: final regressor matrix obtained after stepwise regression).

D. Average model for comparison

To provide a worst-case comparison for the developed LPV model, we defined an *average* model, with a single set of parameters, which we applied to the entire flight envelope to establish to what extent global modelling was needed for the test platform. To account for the non-uniform distribution of the flight data, the average model was obtained by calculating a weighted average

for each parameter in the local model structure from the parameter values of all the local models. Each model parameter was weighted with its distance from the geometric centre $(\bar{V}, \bar{\alpha})$ of the flight envelope, defined as the difference between maximum and minimum V and AOA, respectively, for each of the two spatial coordinates: Each parameter in the average model was thus defined as,

$$\theta_{avg} := \begin{cases} \frac{\sum \theta_k(V_k,\alpha_k) r_k}{\sum r_k} & \text{if} \quad r_k \neq 0 \forall k \\ \theta(\bar{V}, \bar{\alpha}) & \text{if} \quad \exists r_k (r_k = 0) \end{cases}, \qquad r_k := \sqrt{(V_k - \bar{V})^2 + (\alpha_k - \bar{\alpha})^2} \tag{15}$$

where θ represents any parameter in the **A** and **B** matrices defining the model structure (i.e. M_q, M_u, etc.). The second clause of the equation was included to account for the possibility of local models identified at the defined centre of the flight envelope. As no such models were available, effectively only the first clause was used. To ensure a fair comparison also in the validation phase, only the estimation datasets were used to compute the average model.

As discussed previously, a distinction was made between the aerodynamic and purely kinematic components of the LPV model. In an analogous way, two average models were considered. The first is an overall weighted average, defined directly by Eq. 15: here also the kinematic terms are averaged. The second involves averaging only the aerodynamic components according to Eq. 15, while the kinematic terms are assumed to be known in any flight condition. In the evaluations that follow, the latter 'partial average' model is used for comparison (henceforth, this model is termed 'average', while the overall average model is denoted as 'full average'). The results obtained with an overall average were somewhat less accurate than those obtained with a partial average, but mostly in the same order of magnitude. In this sense, comparing the LPV model and partial average can be considered a conservative evaluation of how useful the global model is.

V. LPV modelling results

A. Preliminaries

This section presents the obtained LPV model. Following an assessment of the scheduling results, the final LPV model is evaluated and compared to (i) the original local models, in the conditions where such models are available, (ii) the flight data collected in the same conditions, and (iii) the

'partial' average model presented in Sec. D. Comparing to the local models shows how accurate the LPV model is at reproducing the changing dynamics given by the local models. Comparing to flight data provides additional insight, given that while in theory the best possible outcome is for the LPV model to replicate the local models in the corresponding conditions, in fact it is possible that the LPV model approximates the data better than the local models do, as it does not represent a direct interpolation and may compensate for irregularities in single local models. Finally, comparing to the average model evaluates whether a global model is necessary. Fig. 9 clarifies the relations between the three types of models.

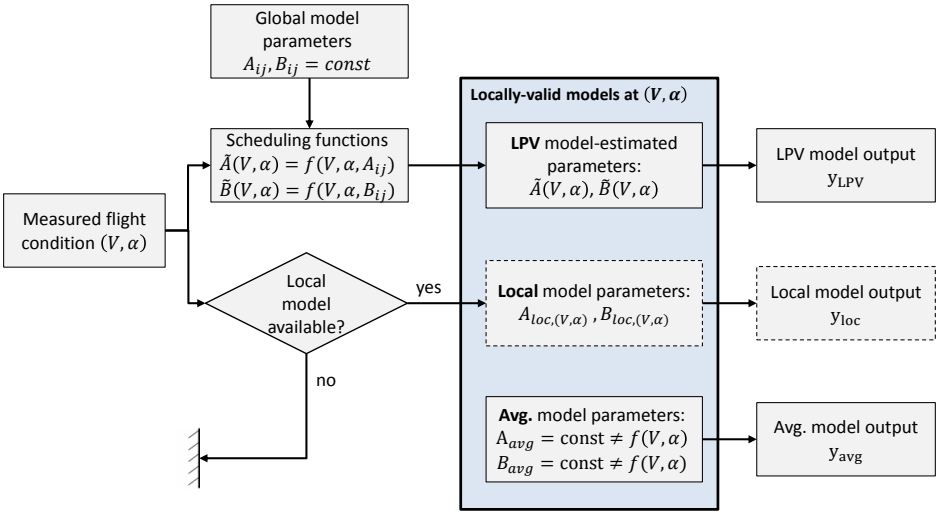

Figure 9: Diagram clarifying the relationship between LPV model, set of local models and average model.

Similarly, it is important to distinguish between (a) global model parameters, (b) LPV model-estimated local parameters, and (c) estimated local parameters. The LPV model contains a set of global parameters (a), which are the same for all flight conditions. The LPV model can be used to estimate local parameters (b): these are the values taken by the left hand side variables in Eqs. 7 and 8 (and all equations analogous to Eq. 9) if AOA and velocity values for a particular flight condition are substituted into the right hand side of the equations. The set of resulting calculated parameters yields an LTI model at the flight condition considered and can therefore be compared to the original local model parameters (c) directly estimated in the same flight condition.

A number of flight test datasets were excluded from the model identification process and used

for validation. For this, nine datasets were selected at random, distributed uniformly among the groups of datasets shown in Fig. 2, in relation to the group size. Different random selections were attempted – given that the outcome remained comparable, suggesting a degree of robustness of the modelling approach, in the remainder of this paper results are shown for one of the estimation-validation selections only (validation datasets: 6, 3, 11, 16, 22, 31, 32, 41, 45; cf. Fig. 2).

B. Scheduling results

Prior to considering the complete LPV model, the estimated local model parameters were evaluated and compared to the corresponding parameters predicted by the LPV model in the same flight conditions. This gave an initial indication of the accuracy of the LPV model and provided further insight into the adequacy of the model structure. Shortcomings in the LPV model are likely to be related to one of the following causes: (i) the parameter is not estimated accurately in the local models, (ii) the chosen scheduling variables are unsuited to represent the variation of the local parameter considered, or (iii) the local parameter is generally unaffected by the flight condition. The first point may be due to insufficient excitation in the identification data, or because the parameter has a limited influence on the system dynamics, or because it is strongly correlated to other parameters and cannot be identified independently from these – these points were addressed in Sec. D. The second point was not considered further, as the local analysis (Sec. III) suggested that the velocity and AOA are suitable to capture the most significant trends in the dynamics. The third point is discussed in this section, in the context of the scheduling results. Based on this evaluation, further minor adjustments were made to the model structure and the final LPV model was obtained.

The approach outlined in Sec. IV was applied, starting from the flight data presented in Sec. C and the local model structure defined in Sec. D (Eq. 2), to obtain an LPV model covering the flight envelope region explored in the current flight tests (cf. Fig. 2). The following scheduling functions were obtained, following the stepwise regression process:

$$\tilde{M}_q = a_{Mq,00} + a_{Mq,10}V + a_{Mq,30}V^3 \tag{16}$$

$$\tilde{M}_u = a_{Mu,00} + a_{Mu,10}V + a_{Mu,20}V^2 + a_{Mu,30}V^3 \tag{17}$$

$$(\tilde{M}_w = \rho_{10}V_0 + \rho_{20}V^2 + \rho_{30}V_0^3 \quad \text{; average used}) \tag{18}$$

$$\tilde{M}_{\delta_e} = b_{M\delta_e,00} + b_{M\delta_e,20}V^2 + b_{M\delta_e,21}V^2\alpha + b_{M\delta_e,30}V^3 \tag{19}$$
$$\tilde{X}_q = a_{Xq,00} + a_{Xq,21}V^2\alpha \tag{20}$$
$$\tilde{X}_u = a_{Xu,00} + a_{Xu,11}V\alpha + a_{Xu,21}V^2\alpha \tag{21}$$
$$\tilde{X}_w = 0 \tag{22}$$
$$\tilde{X}_{\delta_e} = b_{X\delta_e,00} + b_{X\delta_e,10}V + b_{X\delta_e,30}V^3 \tag{23}$$
$$(\hat{Z}_q = \rho_{12}V_0\alpha_0^2 \quad \text{; average used}) \tag{24}$$
$$\tilde{Z}_u = 0 \tag{25}$$
$$\tilde{Z}_w = a_{Xw,00} + a_{Xw,01}\alpha + a_{Xw,11}V\alpha + a_{Xw,12}V\alpha^2 \tag{26}$$
$$\tilde{Z}_{\delta_e} = 0 \tag{27}$$

The bracketed expressions in the equations above denote parameters which were not scheduled in the final model. As discussed above, next to ensuring a sufficient identifiability of the local model parameters at the basis of the global model (cf. Sec. D), the LPV model can be further improved by determining whether the local parameters are in fact significantly related to the flight conditions and only scheduling the parameters that meet this requirement. While the dynamics of the local models are related to the flight condition, this does not necessarily imply that *each* of the local parameters is correlated to the flight condition. Some parameters were found to be important for the system dynamics overall, but either not significantly affected by different flight regimes within the range considered, or difficult to predict with simple functions of the AOA and velocity.

Figs. 10–11 show the local model parameters, the LPV model-estimated parameters for the same flight conditions, and the average model parameters (based on Sec. D). While several parameters depend on both the velocity and AOA, the parameters are plotted against each of these variables separately, to provide a clearer overview. It can be observed that most of the LPV model-calculated parameters take on values close to those of the local models in the same conditions. Where there is a trend with the flight condition, the scheduling sub-models reproduce it accurately, e.g. as clearly seen for M_u, M_{δ_e}, X_q and X_u. The parameters connected to the Z force and w velocity are less accurately predicted by the global model, as expected given their less reliable estimation in the local models. It is also clear that while some parameters display a clear correlation with the flight condition, others display no clear trends even though they are estimated effectively in the local models. This suggests that it is unnecessary to enforce on all local parameters a cor-

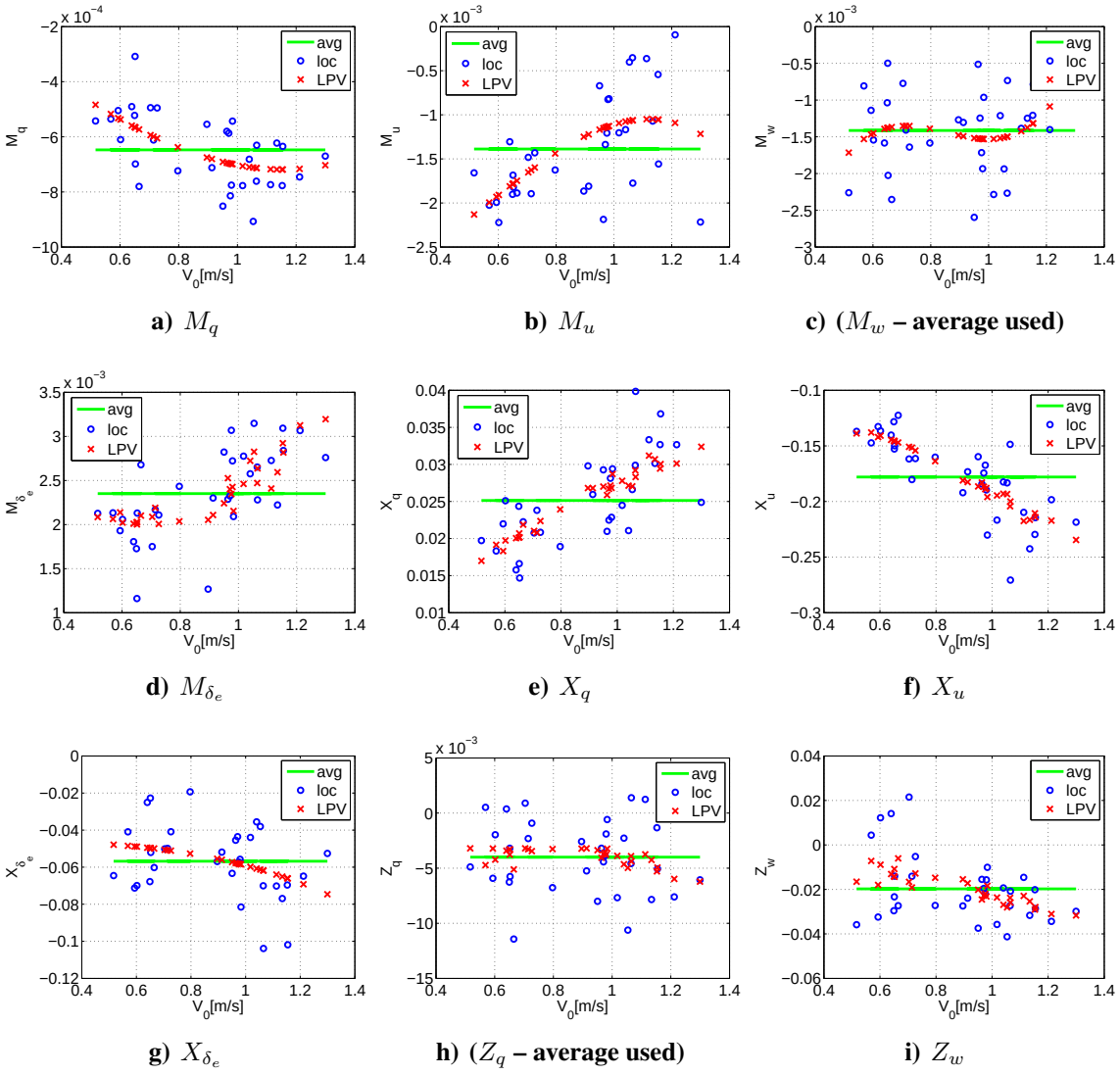

Figure 10: Trim velocity versus: local model parameters, corresponding LPV model-estimated parameters, average model parameters (at conditions in Fig. 2)

relation to the flight condition, and that similar or better results can be obtained by fixing some parameters to constant values and only varying the remaining parameters. This would allow for simpler, smaller models that still capture the main effects. Based on a visual evaluation, the local model parameters M_w and Z_q were found not to vary significantly with the flight regime.

A quantitative evaluation of the accuracy of the LPV model – and of the degree of correlation of local parameters and flight conditions – was also obtained by computing, for each parameter, the correlation between local parameter estimates obtained in all flight conditions and corresponding LPV model-predicted parameters. Additionally, probability values (p-values) were considered to

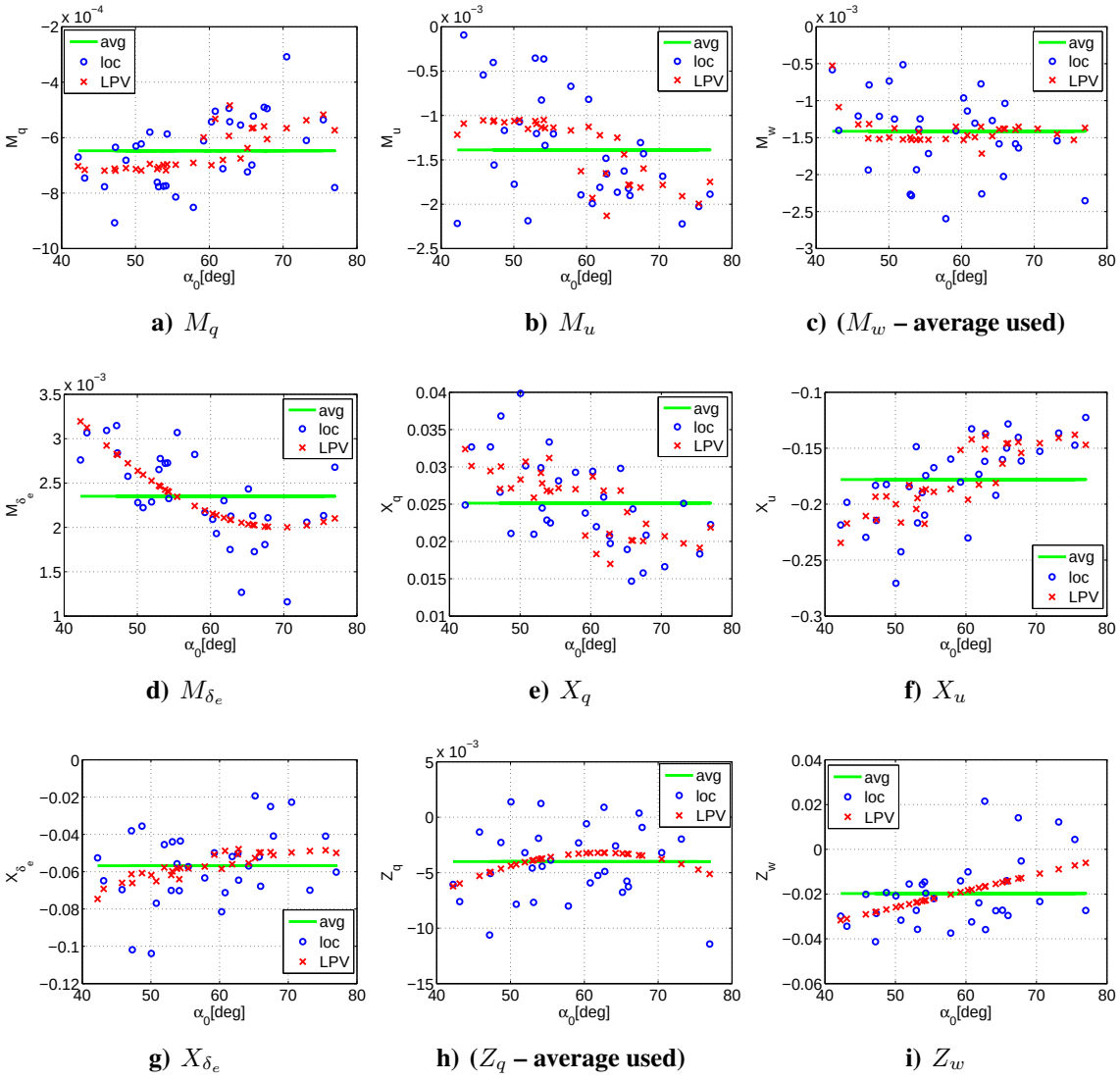

Figure 11: Trim AOA versus: local model parameters, corresponding LPV model-estimated parameters, average model parameters (at conditions in Fig. 2)

evaluate the significance of said correlations. Based on these metrics, shown in Table 4, it was found that most of the parameters in the simplified local model structure are modelled effectively by the chosen LPV formulation, with the exception of M_w and Z_q, which do not display significant trends with the flight condition, and hence are not accurately predicted by the scheduling functions. X_δ and Z_w are also significantly less correlated to the flight conditions compared to the remaining parameters, however the obtained results suggest they may still be possible to model.

On the basis of all the preceding considerations, the parameters M_w and Z_q were fixed to average values (obtained from the average model in Eq. 15. The following LPV model structure

Table 4: Full model structure: correlation (and p-values) between LPV model-estimated parameters and local model parameters.

Param.	$\mathbf{corr}(\tilde{\theta}_{\mathbf{LPV}}, \hat{\theta}_{\mathbf{loc}})$	p-value	Param.	$\mathbf{corr}(\tilde{\theta}_{\mathbf{LPV}}, \hat{\theta}_{\mathbf{loc}})$	p-value	Param.	$\mathbf{corr}(\tilde{\theta}_{\mathbf{LPV}}, \hat{\theta}_{\mathbf{loc}})$	p-value
M_q	0.61	$\ll$0.001	X_q	0.78	$\ll$0.001	Z_q	0.06	0.73
M_u	0.75	$\ll$0.001	X_u	0.83	$\ll$0.001	Z_w	0.55	0.002
M_w	0.22	0.23	X_{δ_e}	0.52	0.003			
M_{δ_e}	0.71	$\ll$0.001						

was thus chosen for the final, simplified (subscript 'simp') global model:

$$\tilde{\mathbf{A}}_{\mathbf{simp}}(V,\alpha) = \begin{bmatrix} \frac{\tilde{M}_q(V)}{I_{yy}} & \frac{\tilde{M}_u(V)}{I_{yy}} & \frac{\bar{M}_w}{I_{yy}} & 0 \\ \frac{\tilde{X}_q(V,\alpha)}{m} - w_0 & \frac{\tilde{X}_u(V,\alpha)}{m} & 0 & g\cos(\Theta_0) \\ \frac{\tilde{Z}_q}{m} + u_0 & 0 & \frac{\tilde{Z}_w(V,\alpha)}{m} & g\sin(\Theta_0) \\ 1 & 0 & 0 & 0 \end{bmatrix}, \tilde{\mathbf{B}}_{\mathbf{simp}}(V,\alpha) = \begin{bmatrix} \frac{\tilde{M}_{\delta_e}(V,\alpha)}{I_{yy}} \\ \frac{\tilde{X}_{\delta_e}(V)}{m} \\ 0 \\ 0 \end{bmatrix} \quad (28)$$

where a bar superscript indicates that the corresponding parameter is fixed to the same constant value (given by Eq. 15) regardless of the flight condition, and not computed from a scheduling function. Note that the parameters in Eq. 28 are estimated from the *global* model, as denoted by the tilde superscript, and can therefore be calculated in any flight condition. The scheduling functions used to obtain the unknown parameters in the above expression were given previously in Eq. 16, except for M_w and Z_q, which are fixed to average values. Substituting the global model parameters into Eq. 16 gives the following final scheduling functions:

$$\tilde{M}_q = -1.49 \times 10^{-4} - 6.98 \times 10^{-4} V + 1.42 \times 10^{-4} V^3 \quad (29)$$
$$\tilde{M}_u = -8.42 \times 10^{-4} - 3.60 \times 10^{-3} V + 3.28 \times 10^{-3} V^2 \quad (30)$$
$$\tilde{M}_w = -1.44 \times 10^{-3} \quad (31)$$
$$\tilde{M}_{\delta_e} = 8.26 \times 10^{-2} + 2.04 \times 10^{-1} V^2 - 0.10 \times 10^{-1} V^2 \alpha - 6.25 \times 10^{-2} V^3 \quad (32)$$
$$\tilde{X}_q = 1.24 \times 10^{-2} + 1.60 \times 10^{-2} V^2 \alpha \quad (33)$$
$$\tilde{X}_u = -1.39 \times 10^{-1} + 8.25 \times 10^{-2} V\alpha - 1.37 \times 10^{-1} V^2 \alpha \quad (34)$$
$$\tilde{X}_w = 0 \quad (35)$$
$$\tilde{X}_{\delta_e} = -1.29 \times 10^{-1} + 1.56 \times 10^{-1} V - 8.10 \times 10^{-2} V^3 \quad (36)$$
$$\tilde{Z}_q = -4.15 \times 10^{-3} \quad (37)$$
$$\tilde{Z}_u = 0 \quad (38)$$
$$\tilde{Z}_w = -3.87 \times 10^{-1} + 3.46 \times 10^{-1} \alpha + 3.67 \times 10^{-1} V\alpha - 3.48 \times 10^{-1} V\alpha^2 \quad (39)$$

$$\tilde{Z}_{\delta_e} = 0 \tag{40}$$

Note that the above equations require the velocity to be given in m/s and the angle of attack in "rad". The simplified model structure was found to yield somewhat improved results, while requiring only approximately half the number of parameters, therefore it represents an attractive solution. Additionally, it improves upon the original model structure in terms of reliability, by only including well-estimated parameters and only scheduling those parameters that vary significantly with the flight condition. The local and global modelling results shown in the remainder of this paper are all based on the simplified model given by Eq. 2. The estimated local parameters are listed in the appendix. Ultimately, rather than by its parameters, a model must be judged by its dynamic properties and the output it predicts. These points are discussed in the next subsections.

C. System dynamics

The resulting model was first evaluated in terms of the system dynamics. This evaluation also provided more detailed insight into the dynamics of the test vehicle, which are therefore discussed further in this section. Fig. 12 shows the poles obtained from the LPV model in the 46 different flight conditions considered, the corresponding 46 local models, and the average model (cf. Sec. D). The poles obtained from each model are also shown separately in Fig. 13, with colour shades illustrating the changes with flight velocity. Lastly, to evaluate each component of the dynamics, the poles of each of the models (or set of models) are plotted separately in Fig. 14, against the flight conditions the LPV model was evaluated at (corresponding to the conditions where local models were available). In the interest of clarity, the complex pole is split into real and imaginary components. Results obtained from validation data are highlighted in the plots. For the sake of clarity, in this section the flight condition is shown only in terms of the velocity – trends with the AOA were in most cases approximately inversely correlated.

As suggested in Sec. B, there are trends between system poles and flight conditions, however this is not the case, to the same extent, for all the poles. The trends that emerged more clearly from the local modelling are replicated accurately by the LPV model, while, as expected, unclear variations in the local modelling results led to unclear global modelling results. This points to

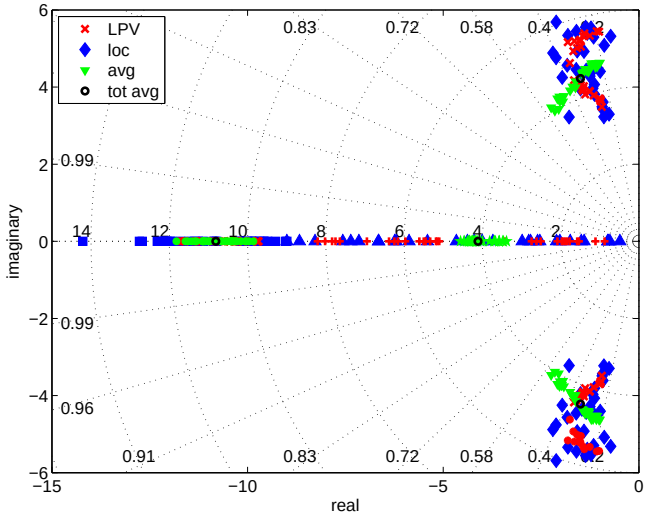

Figure 12: Poles of LPV, local and average models; overall average (with fixed kinematics) also shown.

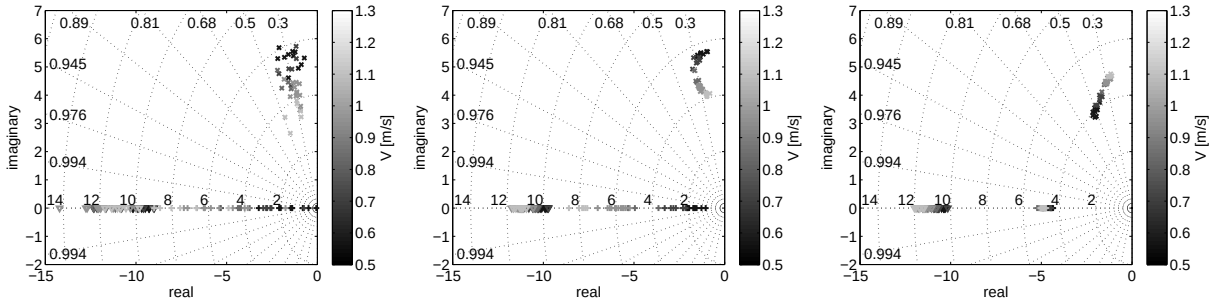

a) Local models **b) LPV model** **c) Average model**

Figure 13: Poles of LPV, local and average models; colour shades indicate changing flight velocity.

shortcomings in the underlying local models rather than in the LPV model.

The complex pole displays a clear trend with the flight condition, as evident from Figs. 14b and 14a, and the corresponding trajectory in Fig. 13. The imaginary component clearly decreases in magnitude at higher velocities, indicating that the frequency decreases. This trend is accurately captured by the LPV model. Interestingly, the average model, which considers the changing kinematics only, shows an opposite trend in the imaginary component, suggesting that the trend seen in the local model oscillatory dynamics (particularly in the frequency) is predominantly determined by the aerodynamics rather than the kinematics. By contrast, the real component of the complex pole displays a considerably smaller overall variation and the local model-obtained values are more scattered, particularly in the low velocity range. Nonetheless, there appears to be a trend, which is

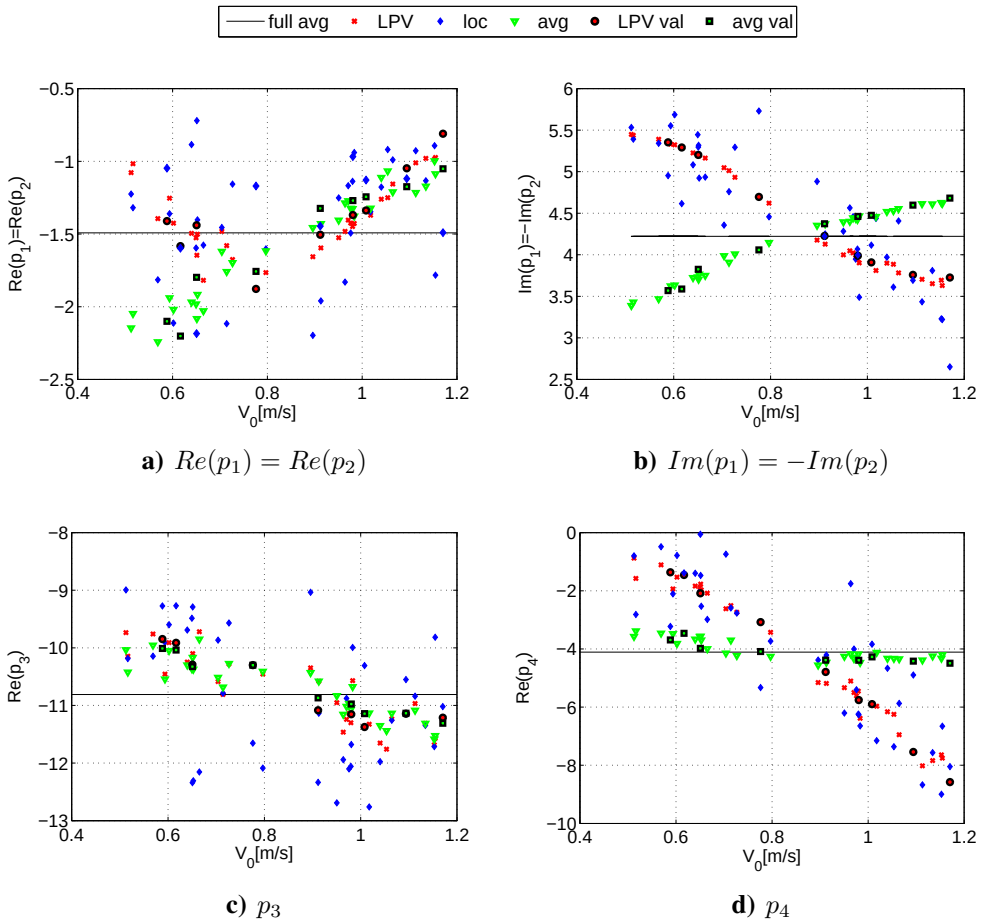

a) $Re(p_1) = Re(p_2)$ **b)** $Im(p_1) = -Im(p_2)$

c) p_3 **d)** p_4

Figure 14: Poles versus corresponding trim velocity: LPV, local and average models (val=validation).

captured by the LPV model, with the damping initially increasing, in the lower velocity range (up to $V \approx 0.8m/s$), and then decreasing again at even higher velocities. The average model displays a very similar result in the high velocity range, but the trend does not reverse at low velocities, suggesting that at low velocities the aerodynamics play a more dominant role in determining the overall dynamic behaviour, compared to the (body) kinematics. There also appears to be a 'sweet spot' for the platform, where the damping is highest – this is in agreement with piloting experience on the FWMAV. However, the significant amount of seemingly random variation in the local data implies that the results for this eigenmode must be verified further.

The faster of the two real poles (p_3) shows only a vague trend, decreasing somewhat at higher velocities, however there is significant variation between the local model results, and further/better data would be required to ascertain this trend. In view of this variation, while the LPV model captures a part of the trend, the result is not clear, especially in the high velocity range. Here,

the LPV and average models are almost identical – this may be because of the parameters that were fixed to constant values or excluded from the model structure, which implies that parts of the LPV model-predicted dynamics (i.e. the parts associated with the Z-force) are very close to those predicted by the average model. Despite the somewhat unclear result, it should be noted that since this is the fastest pole, it should play a limited part in the overall response. The slower pole (p_4) displays a very clear trend with the flight condition, which is captured with accuracy by the LPV model. The average model, by contrast, barely captures this trend, suggesting that this component of the dynamics too is determined by the aerodynamics rather than the kinematics. It can also be seen that this pole becomes unstable at very low velocities and clearly unstable at hover.

Overall, the damping decreases at low velocities. At higher velocities, the real poles become more negative but the oscillatory pole seems to eventually become unstable. The oscillatory component decreases in frequency, in agreement with the observed flight behaviour of the FWMAV. The significant differences between LPV and average model trends suggest that the aerodynamics indeed change with changing flight conditions, and that they influence the overall flight behaviour more than the kinematics. Overall the LPV model is accurate in capturing the trends emerging from the data and can be used to predict the changing system dynamics in different conditions. Further effects may become evident with new identification data where the linear velocity dynamics are better excited – this may provide more insight on the fast aperiodic pole p_3.

D. Output match

Figs. 15 and 16 show examples of the output predicted by the LPV model, compared to the flight data, the output of the corresponding local models, and the output of the average model. Result examples are shown for both estimation and validation datasets, with the specific datasets selected from different parts of the flight envelope so as to present a basic overview. A more comprehensive overview is given in Figs. 17–19, which show statistical metrics (RMS errors and output correlation coefficients) evaluating the performance of the LPV model for all datasets. These figures also show the difference in performance, respectively, between LPV and average models, and between LPV and local models. The same information is also summarised in Table 5.

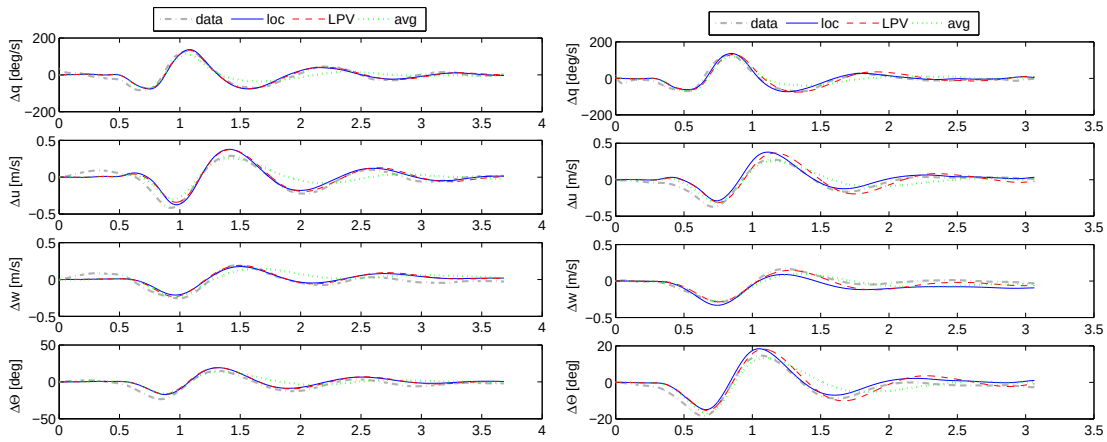

a) Test #2 (low velocity/ high AOA condition) **b) Test #14 (low velocity/high AOA condition)**

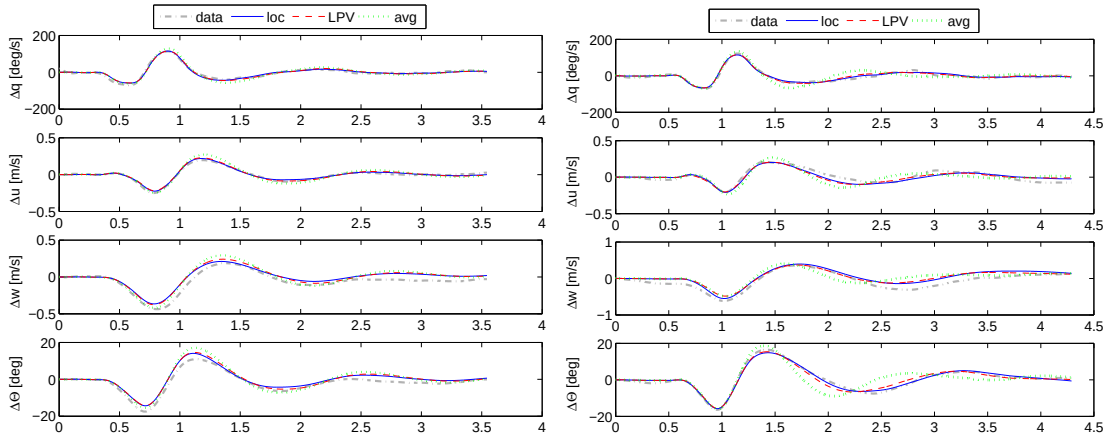

c) Test #26 (intermediate velocity/AOA condition) **d) Test #38 (high velocity/ low AOA condition)**

Figure 15: Output example: LPV, average and local models, versus flight data (estimation sets)

As anticipated from the scheduling results (Sec. B), the LPV model approximates the flight data effectively, reaching a high accuracy in both the estimation and the validation tests. The validation results, in particular, suggest that the model can be used to predict the flight behaviour where no local models are available. While the local models are consistently more accurate than the LPV results computed in the same conditions – as expected, given that the local models were used to construct the LPV model and considered correct a priori – the differences between the set of local models and the LPV model are small. There are also isolated cases where the LPV model displays a marginally better performance than the corresponding local model (cf. Fig. 19) – these are cases where the relevant local model is less accurate, e.g. due to less clean identification data, suggesting that the LPV model is more dependable and can help to circumvent locally inaccurate models.

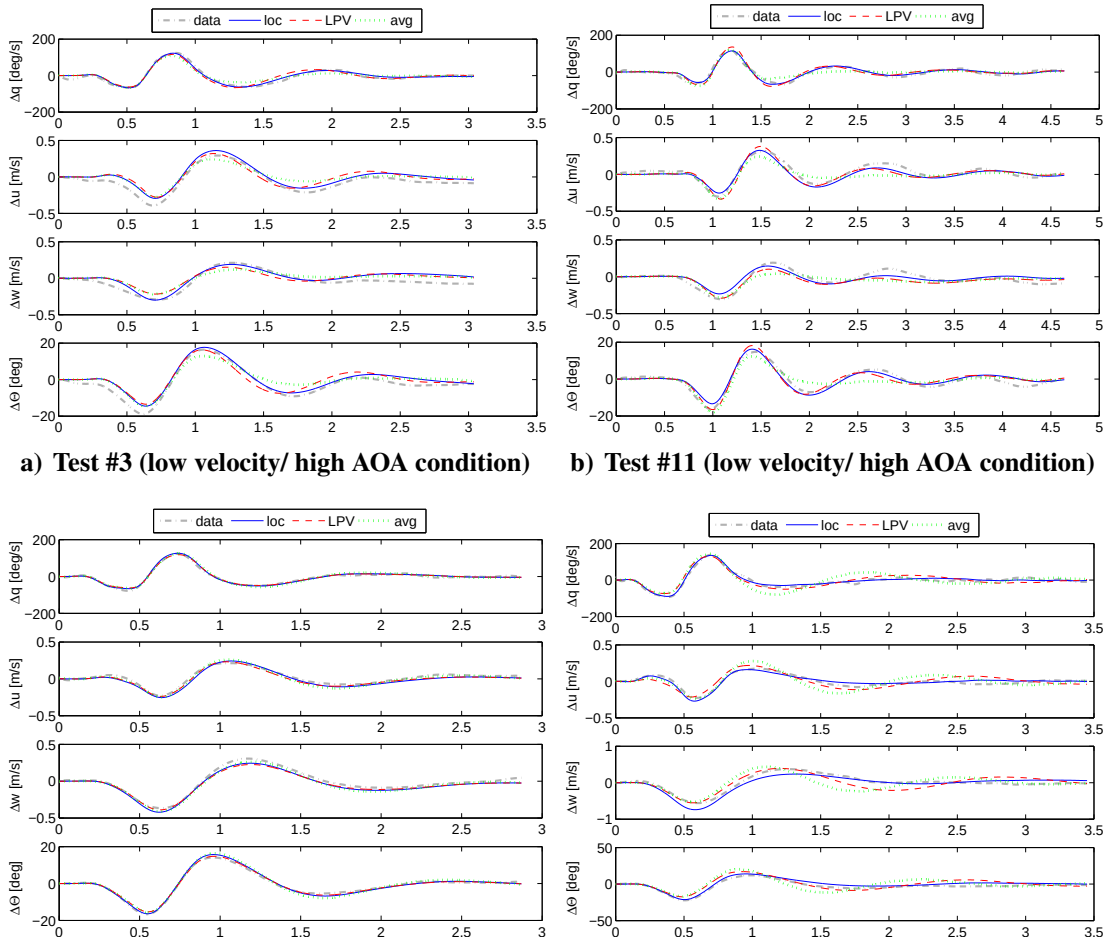

a) Test #3 (low velocity/ high AOA condition)

b) Test #11 (low velocity/ high AOA condition)

c) Test #22 (intermediate velocity/AOA condition)

d) Test #45 (high velocity/ low AOA condition)

Figure 16: Output example: simplified LPV, average and local models, versus flight data (validation sets)

The LPV model is accurate and scalable, and hence brings a significant improvement compared to the use of a single average model. Fig. 18 highlights that the LPV model consistently achieves a higher accuracy than the average model (cf. also Figs. 15 and 16). While the differences are of a small magnitude, the small scale of the entire problem implies that seemingly negligible changes may have a significant effect, as discussed in Sec. III. This also means that the achievable modelling accuracy is limited and emphasises the effect of inaccuracies in the scheduling. Indeed, it can be remarked that although the LPV scheduling is effective overall and yields results (parameters and eigenvalues) significantly closer to the local results than the average model (cf. Secs. B and refsec: results dynamics), the difference in the resulting output is less noticeable. It appears that the modelling errors involved are large enough to affect the final result, even though per se they

appear to be small, and the main trends are replicated accurately by the LPV model.

Table 5: Percentage of considered conditions where LPV model performs better than average/local models.

	RMSE: % cases better than				corr: % cases better than			
State	**Avg.(est.)**	**Loc.(est.)**	**Avg.(val.)**	**Loc.(val.)**	**Avg.(est.)**	**Loc.(est.)**	**Avg.(val.)**	**Loc.(val.)**
q	87	10	100	11	84	6	100	11
u	81	6	89	11	77	6	67	11
w	81	10	44	0	77	13	67	11
Θ	84	10	100	0	81	16	100	0

Overall, the LPV model is accurate and offers several advantages over both the average model and the set of local models. Unlike the average model, the LPV model does not deteriorate in accuracy as the flight conditions change. Figs. 18 and 19 show that in the central part of the flight envelope the LPV and average model results are similar, but that the average model increasingly loses accuracy at flight conditions increasingly different from those in the middle of the envelope. This can also be seen in the output (Fig. 15): especially at low velocities, the discrepancy between average model and flight data is clear. This effect would become more pronounced if a wider flight envelope were considered (e.g. through changes to the vehicle configuration), hence an average model is not a robust solution, and is inadequate for high-accuracy applications.

By contrast, the LPV model retains a similar performance throughout the domain considered, with the exception of isolated outliers, whose decreased performance can be traced back to the estimation data. It represents a scalable solution that can be extended to cover a vaster flight envelope, and can be used effectively to predict how the system dynamics change. While less accurate than the local models – as expected, since the estimation process minimises the difference between LPV model and closest local model –, the LPV model has the advantages of higher flexibility, continuous coverage and a smaller overall model size (a total of 25 parameters, as opposed to 12 parameters per flight condition). Additionally, whereas single local models may be inaccurate, e.g. due to inaccurate identification data, if the majority of the original local models are accurate, the LPV model can bypass local errors in favour of the more significant overall trends.

The modelling approach itself is therefore considered effective and useful when dealing with FWMAVs that can be locally represented by LTI models (the most widespread formulation in the

literature). Whether the suggested approach remains effective when considering more significant variation (e.g. including the effect of CG shifts, which would allow for higher velocities) must be verified, however the approach remains theoretically applicable. The fact that the LPV model remains accurate at the edges of the considered region suggests that some further extrapolation could be handled. More generally, the LPV approach has the advantage of simplicity, in both the model structure and the identification requirements.

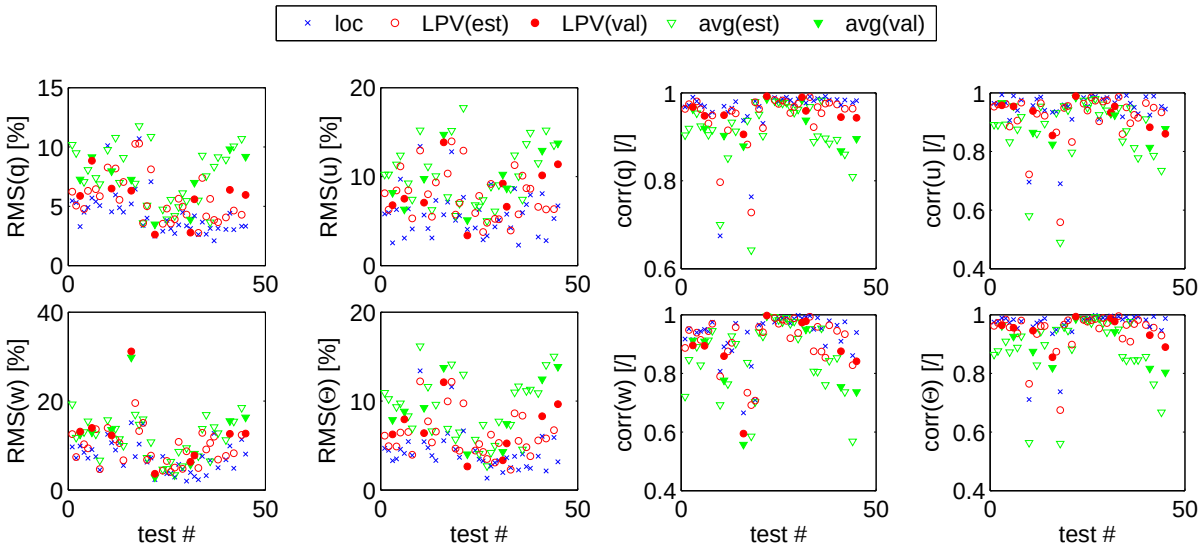

Figure 17: LPV, average and local model-obtained results, compared to flight test data.

VI. Conclusions

A linear parameter-varying (LPV) model identification approach was developed to represent the time-averaged longitudinal dynamics of a flapping-wing micro aerial vehicle. This involved, firstly, estimating local models of the dynamics, using 46 sets of free-flight data collected in different flight conditions, and, secondly, determining a set of scheduling functions to express the dependency of these models on the flight condition they represent. The obtained scheduling functions accurately model the key dynamic properties of the vehicle, and hence constitute a useful means of predicting and simulating the system dynamics in different flight conditions. With a significantly lower number of parameters, the global model achieves an only slightly lower accuracy than the set of local models, while additionally providing continuous coverage across the condi-

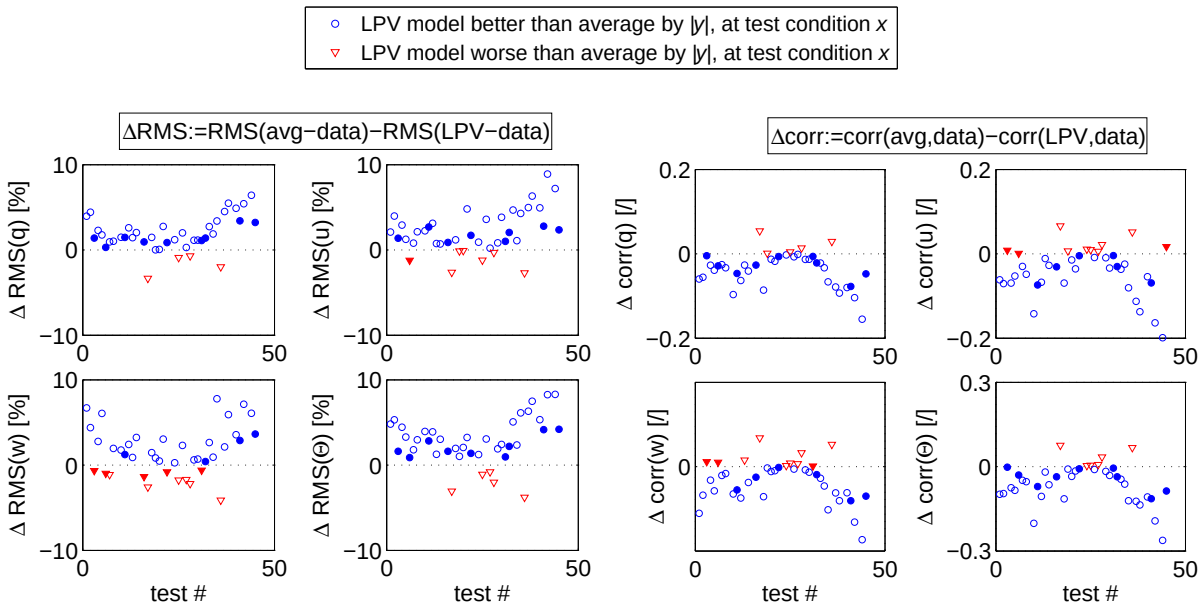

Figure 18: LPV and average model-obtained results, compared to flight data (validation sets: filled markers)

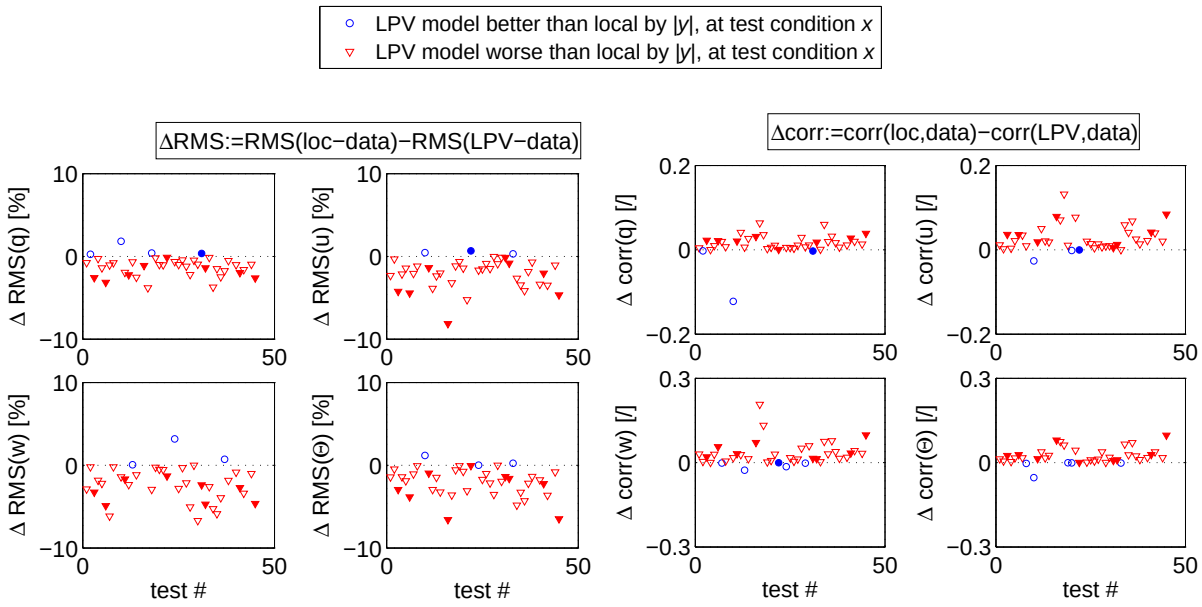

Figure 19: LPV and local model-obtained results, compared to flight data (validation sets: filled markers).

tions considered, and thus also increased flexibility. The model requires few measurements, and is computationally light and easily interpretable. These properties make it suitable for simulation and control work. Moreover, the model retains an approximately constant accuracy up to the edges of the covered flight envelope, suggesting that some extrapolation is possible and that the approach

may remain effective to represent more significant variation, provided linear models remain effective locally. The modelling process also yielded information on the dynamics of the test vehicle, showing that these vary with the angle of attack and flight velocity and providing insight into how they vary. The observed trends are consistent with flight experience, corroborating the obtained results. Improved results may be obtainable with more informative and extensive flight data, leading to more accurate local models and hence a more accurate global model. The suggested approach is also applicable to account for different vehicle configurations in a single model: this type of extension would involve larger changes and hence more fully exploit the LPV approach.

References

[1] Ellington, C. P., "The Aerodynamics of Hovering Insect Flight. I. The Quasi-Steady Analysis," *Philosophical Transactions of the Royal Society B: Biological Sciences*, Vol. 305, No. 1122, 1984, pp. 1–15. doi:10.1098/rstb.1984.0049.

[2] Ellington, C. P., van den Berg, C., Willmott, A. P., and Thomas, A. L. R., "Leading-edge vortices in insect flight," *Nature*, Vol. 384, 1996, pp. 626–630. doi:10.1038/384626a0.

[3] Dickinson, M. H., Lehmann, F.-O., and Sane, S. P., "Wing Rotation and the Aerodynamic Basis of Insect Flight," *Science*, Vol. 284, No. 5422, 1999, pp. 1954–1960. doi:10.1126/science.284.5422.1954.

[4] Taylor, G. K. and Thomas, A. L. R., "Dynamic flight stability in the desert locust Schistocerca gregaria," *Journal of Experimental Biology*, Vol. 206, No. 16, Aug. 2003, pp. 2803–2829. doi:10.1242/jeb.00501.

[5] Grauer, J., Ulrich, E., Hubbard, J. E., Pines, D., and Humbert, J. S., "Testing and System Identification of an Ornithopter in Longitudinal Flight," *Journal of Aircraft*, Vol. 48, No. 2, March 2011, pp. 660–667. doi:10.2514/1.C031208.

[6] Caetano, J. V., de Visser, C. C., de Croon, G. C. H. E., Remes, B., De Wagter, C., and Mulder, M., "Linear Aerodynamic Model Identification of a Flapping Wing MAV Based on Flight Test Data," *Int. Journal of Micro Air Vehicles*, 2013. doi:10.1260/1756-8293.5.4.273.

[7] Armanini, S. F., de Visser, C. C., and de Croon, G. C. H. E., "Black-box LTI Modelling of Flapping-wing Micro Aerial Vehicle Dynamics," *AIAA Atmospheric Flight Mechanics Conf.*, 2015, AIAA Paper 15-0234. doi:10.2514/6.2015-0234.

[8] Berman, G. J. and Wang, Z. J., "Energy-minimizing kinematics in hovering insect flight," *Journal of Fluid Mechanics*, Vol. 582, 2007, pp. 153–168. doi:10.1017/S0022112007006209.

[9] Orlowski, C. T. and Girard, A. R., "Averaging of the Nonlinear Dynamics of Flapping Wing Micro Air Vehicles for Symmetrical Flapping," *AIAA Journal*, Vol. 49, No. 5, 2011, pp. 969–981. doi:10.2514/1.J050649.

[10] Khan, Z. A. and Agrawal, S. K., "Force and moment characterization of flapping wings for micro air vehicle application," *American Control Conf.*, 2005, pp. 1515–1520. doi:10.1109/ACC.2005.1470180.

[11] Xiong, Y. and Sun, M., "Stabilization control of a bumblebee in hovering and forward flight," *Acta Mechanica Sinica*, Vol. 25, No. 1, 2009, pp. 13–21. doi:10.1007/s10409-008-0184-8.

[12] Wu, J. and Sun, M., "Control for going from hovering to small speed flight of a model insect," *Acta Mechanica Sinica*, Vol. 25, No. 3, 2009, pp. 295–302. doi:10.1007/s10409-009-0241-y.

[13] Finio, B. M., Perez-Arancibia, N. O., and Wood, R. J., "System identification and linear time-invariant modeling of an insect-sized flapping-wing micro air vehicle," *2011 IEEE/RSJ Int. Conf. on Intelligent Robots and Systems*, 2011, pp. 1107–1114. doi:10.1109/IROS.2011.6094421.

[14] Duan, H. and Li, Q., "Dynamic model and attitude control of Flapping Wing Micro Aerial Vehicle," *IEEE Int. Conf. on Robotics and Biomimetics (ROBIO)*, Dec. 2009, pp. 451–456. doi:10.1109/ROBIO.2009.5420689.

[15] Chand, A. N., Kawanishi, M., and Narikiyo, T., "Parameter Estimation for the Pitching Dynamics of a Flapping-Wing Flying Robot," *IEEE Int. Conf. on Advanced Intelligent Mechatronics (AIM)*, 2015, pp. 1552–1558. doi:10.1109/AIM.2015.7222763.

[16] Armanini, S. F., de Visser, C. C., de Croon, G. C. H. E., and Mulder, M., "Time-varying model identification of flapping-wing vehicle dynamics using flight data," *Journal of Guidance, Control, and Dynamics*, Vol. 39, No. 3, 2016, pp. 526–541. doi:10.2514/1.G001470.

[17] Sename, O., Gáspár, P., and Bokor, J., editors, *Robust Control and Linear Parameter Varying Approaches*, Lecture Notes in Control and Information Sciences, Springer, Berlin Heidelberg, 2013. doi:10.1007/978-3-642-36110-4.

[18] Tóth, R., Van den Hof, P. M. J., Ludlage, J. H. a., and Heuberger, P. S. C., "Identification of nonlinear process models in an LPV framework," *Proceedings of the 9th International Symposium on Dynamics and Control of Process Systems*, 2010, pp. 869–874. doi:10.3182/20100705-3-BE-2011.00145.

[19] Leith, D. J. and Leithead, W. E., "Survey of Gain-Scheduling Analysis and Design," *International Journal of Control*, Vol. 73, No. 11, 2000, pp. 1001–1025. doi:10.1080/002071700411304.

[20] Morelli, E. A., "Global Nonlinear Aerodynamic Modeling using Multivariate Orthogonal Functions," *Journal of Aircraft*, Vol. 32, No. 2, 1995. doi:10.2514/3.46712.

[21] Brandon, J. M. and Morelli, E. A., "Real-Time Onboard Global Nonlinear Aerodynamic Modeling from Flight Data," *Journal of Aircraft*, Vol. 53, No. 5, 2016. doi:10.2514/1.C033133.

[22] de Visser, C. C., Mulder, J. A., and Chu, Q. P., "Global Nonlinear Aerodynamic Model Identification with Multivariate Splines," *AIAA Atmospheric Flight Mechanics Conf.*, 2009, AIAA paper 2009-5726. doi:10.2514/6.2009-5726.

[23] Fujimori, A. and Ljung, L., "Model identification of linear parameter varying aircraft systems," *IMechE Part G: J. Aerospace Engineering*, Vol. 220, 2006. doi:10.1243/09544100JAERO28.

[24] Marcos, A. and Balas, G. J., "Development of Linear-Parameter-Varying Models for Aircraft," *Journal of Guidance, Control, and Dynamics*, Vol. 27, No. 2, 2004, pp. 218–228. doi:10.2514/1.9165.

[25] Marcos, A., Veenman, J., Scherer, C. W., De Zaiacomo, G., Mostaza, D., Kerr, M., Kroglu, H., and Bennani, S., "Application of LPV Modeling, Design and Analysis Methods to a Re-entry Vehicle," *AIAA Guidance, Navigation and Control Conference*, No. 2010-8192, 2010. doi:10.2514/6.2010-8192.

[26] Balas, G. J., Fiahlo, I., Packard, A., Renfrow, J., and Mullaney, C., "On the Design of the LPV Controllers for the F-14 Aircraft Lateral-Directional Axis During Powered Approach," *American Control Conf.*, 1997. doi:10.2514/2.4323.

[27] Seiler, P., Balas, G., and Packard, A., *Control of Linear Parameter Varying Systems with Applications*, chap. Linear parameter varying control for the X-53 active aeroelastic wing, Springer, Boston, MA, 2012. doi:10.1007/978-1-4614-1833-7_19.

[28] Westermayer, C., Schirrer, A., Hemedi, M., and Kozek, M., "Linear parameter-varying control of a large blended wing body flexible aircraft," *IFAC Proceedings*, Vol. 43, 2010, pp. 19–24. doi:10.3182/20100906-5-JP-2022.00005.

[29] Weilai, J., Chaoyang, D., and Qing, W., "A systematic method of smooth switching LPV controllers design for a morphing aircraft," *Chinese Journal of Aeronautics*, Vol. 28, No. 6, 2015, pp. 1640–1649. doi:10.1016/j.cja.2015.10.005.

[30] Berger, T., Tischler, M., Hagerott, S. G., Cotting, M. C., Gray, W. R., Gresham, J. L., George, J. E., Krogh, K. J., D'Argeniok, A., and Howland, J. D., "Development and Validation of a Flight-Identified Full-Envelope Business Jet Simulation Model Using a Stitching Architecture," *AIAA Modeling and Simulation Technologies Conf.*, 2017. doi:10.2514/6.2017-1550.

[31] Klein, V. and Morelli, E. A., *Aircraft System Identification: Theory And Practice*, AIAA Education Series, Reston, VA, 2006, ISBN: 1-56347-832-3.

[32] de Croon, G. C. H. E., Perçin, M., Remes, B. D. W., Ruijsink, R., and De Wagter, C., *The DelFly Design, Aerodynamics, and Artificial Intelligence of a Flapping Wing Robot*, Springer Netherlands, 2016, ISBN 978-94-017-9208-0.

[33] de Croon, G. C. H. E., de Clercq, K. M. E., Ruijsink, R., Remes, B. D. W., and de Wagter, C., "Design, aerodynamics, and vision-based control of the DelFly," *Int. Journal of Micro Air Vehicles*, Vol. 1, No. 2, 2009, pp. 71–98. doi:10.1260/175682909789498288.

[34] Armanini, S. F., Karásek, M., E., d. G. C. H., and de Visser, C. C., "Onboard/ offboard sensor fusion for high-fidelity flapping-wing robot flight data," *Journal of Guidance, Control and Dynamics*, Vol. 40, No. 8, 2017. doi:10.2514/1.G002527.

[35] Armanini, S. F., Karásek, M., de Visser, C. C., de Croon, G. C. H. E., and Mulder, M., "Flight testing and preliminary analysis for global system identification of ornithopter dynamics using on-board and off-board data," *AIAA Atmospheric Flight Mechanics Conf.*, 2017, AIAA Paper 2017-1634. doi:10.2514/6.2017-1634.

[36] Karásek, M., Koopmans, A. J., Armanini, S. F., Remes, B. D. W., and de Croon G. C. H. E., "Free Flight Force Estimation of a 23.5 g Flapping Wing MAV using an on-board IMU," *Int. Conf. on intelligent robots and systems (IROS)*, 2016. doi:10.1109/IROS.2016.7759729.

[37] Caetano, J. V., de Visser, C. C., Remes, B. D., De Wagter, C., Van Kampen, E.-J., and Mulder, M., "Controlled Flight Maneuvers of a Flapping Wing Micro Air Vehicle: a Step Towards the Delfly II Identification," *AIAA Atmospheric Flight Mechanics Conf.*, 2013. doi:10.2514/6.2013-4843, AIAA Paper 2013-4843.

[38] Orlowski, C., Girard, A., and Shyy, W., "Derivation and simulation of the nonlinear dynamics of a flapping wing micro-air vehicle," *European Micro Aerial Vehicle Conference and Flight Competition*, 2009, www.imavs.org/papers/2009/33_EMAV09.pdf.

[39] Bolender, M. A., "Rigid Multi-Body Equations-of-Motion for Flapping Wing MAVs using Kane Equations," *AIAA Guidance, Navigation, and Control Conf.*, No. 2009-6158, Aug. 2009. doi:10.2514/6.2009-6158.

[40] Grauer, J. A., Hubbard, J. E., and Jr, J. E. H., "Multibody Model of an Ornithopter," *Journal of Guidance, Control, and Dynamics*, Vol. 32, No. 5, 2009, pp. 1675–1679. doi:10.2514/1.43177.

[41] Sun, M. and Xiong, Y., "Dynamic flight stability of a hovering bumblebee." *Journal of Experimental Biology*, Vol. 208, No. Pt 3, Feb. 2005, pp. 447–59. doi:10.1242/jeb.01407.

[42] Faruque, I. and Sean Humbert, J., "Dipteran insect flight dynamics. Part 1 Longitudinal motion about hover." *Journal of theoretical biology*, Vol. 264, No. 2, 2010, pp. 538–52. doi:10.1016/j.jtbi.2010.02.018.

[43] Caetano, J. V., Armanini, S. F., and Karásek, M., "In-flight data acquisition and flight testing for system identification of flapping-wing MAVs," *IEEE Int. Conf. on Unmanned Aerial Systems (ICUAS)*, 2017. doi:10.1109/ICUAS.2017.7991452.

[44] Mulder, J., *Design and evaluation of dynamic flight test manoeuvres*, Phd, Delft University of Technology, 1986.

[45] Morelli, E., "Flight test validation of optimal input design and comparison to conventional inputs," *AIAA Atmospheric Flight Mechanics Conf.*, 1997, AIAA Paper 1997-3711. doi:10.2514/6.1997-3711.

[46] Papageorgiou, G., Glover, K., D'Mello, G., and Patel, Y., "Taking robust LPV control into flight on the VAAC Harrier," *39th IEEE Conf. on Decision and Control*, Vol. 5, 2000, pp. 4558–4564. doi:10.1109/CDC.2001.914633.

[47] Hammoudi, M. N. and Lowenberg, M. H., "Dynamic gain scheduled control of an F16 model," *AIAA Guidance, Navigation and Control Conf.*, 2008, AIAA Paper 2008-6487. doi:10.2514/6.2008-6487.

[48] Bamieh, B. and Giarré, L., "Identification of linear parameter varying models," *Int. Journal of Robust and Nonlinear Control*, Vol. 12, No. 9, 2002, pp. 841–853. doi:10.1002/rnc.706.

[49] Tóth, R., *Modeling and Identification of Linear Parameter-Varying Systems an Orthonormal Basis Function Approach*, Phd thesis, Delft University of Technology, 2008.

[50] Jategaonkar, R., *Flight Vehicle System Identification A Time Domain Methodology*, AIAA Progress in Astronautics and Aeronautics, Reston, VA, USA, 2006, ISBN: 1-56347-836-6.

[51] Klein, V. and Batterson, J. G., "Determination of airplane model structure from flight data using splines and stepwise regression," Tech. Paper 2126, NASA, 1983.

Appendix: Local model parameters and test conditions

Table 6: Flight test trim conditions

test #	$V[m/s]$	$\alpha[deg]$	$f_f[Hz]$	test #	$V[m/s]$	$\alpha[deg]$	$f_f[Hz]$	test #	$V[m/s]$	$\alpha[deg]$	$f_f[Hz]$	test #	$V[m/s]$	$\alpha[deg]$	$f_f[Hz]$
1	0.52	62.78	13.78	13	0.57	75.44	13.60	25	0.97	54.29	12.77	37	1.05	47.17	12.13
2	0.59	60.80	13.79	14	0.60	73.15	14.26	26	0.91	61.83	12.33	38	1.11	54.13	11.79
3	0.62	73.41	13.57	15	0.79	61.85	13.39	27	0.98	53.80	12.93	39	1.07	50.06	12.23
4	0.65	65.97	13.99	16	0.78	67.55	13.92	28	1.02	53.13	12.87	40	1.13	50.78	12.10
5	0.51	73.68	15.15	17	0.70	62.67	13.28	29	0.98	55.44	12.39	41	1.09	53.02	12.01
6	0.65	66.78	13.33	18	0.73	67.84	12.85	30	0.96	51.94	12.42	42	1.15	45.80	12.30
7	0.67	76.99	13.13	19	0.80	65.17	13.00	31	0.98	55.09	12.30	43	1.21	49.34	12.23
8	0.65	65.77	13.74	20	0.71	59.23	14.02	32	1.01	52.49	12.21	44	1.21	43.12	12.39
9	0.65	77.01	13.86	21	0.90	64.23	11.97	33	1.04	48.70	12.56	45	1.17	50.36	12.31
10	0.65	70.48	13.35	22	0.91	56.53	12.55	34	0.98	60.29	12.12	46	1.30	42.23	12.43
11	0.59	74.09	13.27	23	0.98	52.88	12.65	35	1.15	47.29	12.52				
12	0.64	67.42	13.74	24	0.95	57.84	12.45	36	1.06	52.95	12.47				

Table 7: Simplified local model: estimated parameters and standard deviations ($\hat{\theta}(\hat{\sigma})$), cf. Eq. 2

Param.	Model # 1	2	3	4
$\mathbf{M_q}$	$-5.43 \times 10^{-4}(3.89 \times 10^{-6})$	$-5.05 \times 10^{-4}(2.63 \times 10^{-6})$	$-5.26 \times 10^{-4}(2.28 \times 10^{-6})$	$-5.22 \times 10^{-4}(3.00 \times 10^{-6})$
$\mathbf{M_u}$	$-1.66 \times 10^{-3}(2.78 \times 10^{-5})$	$-1.99 \times 10^{-3}(1.59 \times 10^{-5})$	$-1.27 \times 10^{-3}(1.00 \times 10^{-5})$	$-1.90 \times 10^{-3}(2.01 \times 10^{-5})$
$\mathbf{M_w}$	$-2.26 \times 10^{-3}(6.44 \times 10^{-5})$	$-1.14 \times 10^{-3}(3.68 \times 10^{-5})$	$-1.35 \times 10^{-3}(1.31 \times 10^{-5})$	$-1.04 \times 10^{-3}(3.85 \times 10^{-5})$
$\mathbf{M_{\delta_e}}$	$2.13 \times 10^{-3}(1.77 \times 10^{-5})$	$1.93 \times 10^{-3}(1.38 \times 10^{-5})$	$2.12 \times 10^{-3}(1.13 \times 10^{-5})$	$1.73 \times 10^{-3}(1.34 \times 10^{-5})$
$\mathbf{X_q}$	$1.97 \times 10^{-2}(1.49 \times 10^{-4})$	$2.20 \times 10^{-2}(1.24 \times 10^{-4})$	$2.10 \times 10^{-2}(8.10 \times 10^{-5})$	$2.44 \times 10^{-2}(2.26 \times 10^{-4})$
$\mathbf{X_u}$	$-1.37 \times 10^{-1}(5.40 \times 10^{-4})$	$-1.33 \times 10^{-1}(4.33 \times 10^{-4})$	$-1.45 \times 10^{-1}(2.96 \times 10^{-4})$	$-1.28 \times 10^{-1}(7.97 \times 10^{-4})$
$\mathbf{X_{\delta_e}}$	$-6.45 \times 10^{-2}(7.98 \times 10^{-4})$	$-7.12 \times 10^{-2}(6.06 \times 10^{-4})$	$-4.60 \times 10^{-2}(4.29 \times 10^{-4})$	$-6.78 \times 10^{-2}(1.02 \times 10^{-3})$
$\mathbf{Z_q}$	$-4.89 \times 10^{-3}(1.74 \times 10^{-4})$	$-5.92 \times 10^{-3}(1.36 \times 10^{-4})$	$7.86 \times 10^{-5}(1.80 \times 10^{-4})$	$-6.26 \times 10^{-3}(2.13 \times 10^{-4})$
$\mathbf{Z_w}$	$-3.59 \times 10^{-2}(1.18 \times 10^{-3})$	$-3.24 \times 10^{-2}(8.76 \times 10^{-4})$	$8.30 \times 10^{-3}(5.41 \times 10^{-4})$	$-2.96 \times 10^{-2}(1.50 \times 10^{-3})$

Param.	Model # 5	6	7	8
$\mathbf{M_q}$	$-4.88 \times 10^{-4}(1.96 \times 10^{-6})$	$-7.55 \times 10^{-4}(4.06 \times 10^{-6})$	$-7.80 \times 10^{-4}(7.29 \times 10^{-6})$	$-6.99 \times 10^{-4}(4.59 \times 10^{-6})$
$\mathbf{M_u}$	$-1.69 \times 10^{-3}(1.30 \times 10^{-5})$	$-2.88 \times 10^{-3}(1.19 \times 10^{-5})$	$-1.89 \times 10^{-3}(2.06 \times 10^{-5})$	$-1.82 \times 10^{-3}(1.56 \times 10^{-5})$
$\mathbf{M_w}$	$-1.25 \times 10^{-3}(2.84 \times 10^{-5})$	$-2.14 \times 10^{-4}(1.43 \times 10^{-5})$	$-2.35 \times 10^{-3}(3.72 \times 10^{-5})$	$-2.03 \times 10^{-3}(2.35 \times 10^{-5})$
$\mathbf{M_{\delta_e}}$	$1.85 \times 10^{-3}(1.01 \times 10^{-5})$	$2.56 \times 10^{-3}(1.19 \times 10^{-5})$	$2.68 \times 10^{-3}(2.45 \times 10^{-5})$	$2.13 \times 10^{-3}(1.52 \times 10^{-5})$
$\mathbf{X_q}$	$2.10 \times 10^{-2}(2.65 \times 10^{-4})$	$2.02 \times 10^{-2}(1.24 \times 10^{-4})$	$2.23 \times 10^{-2}(1.99 \times 10^{-4})$	$1.47 \times 10^{-2}(1.43 \times 10^{-4})$
$\mathbf{X_u}$	$-1.14 \times 10^{-1}(8.32 \times 10^{-4})$	$-1.26 \times 10^{-1}(5.07 \times 10^{-4})$	$-1.23 \times 10^{-1}(6.71 \times 10^{-4})$	$-1.50 \times 10^{-1}(5.64 \times 10^{-4})$
$\mathbf{X_{\delta_e}}$	$-5.78 \times 10^{-2}(8.49 \times 10^{-4})$	$-4.24 \times 10^{-2}(4.80 \times 10^{-4})$	$-6.02 \times 10^{-2}(8.05 \times 10^{-4})$	$-5.20 \times 10^{-2}(5.64 \times 10^{-4})$
$\mathbf{Z_q}$	$-9.73 \times 10^{-4}(1.33 \times 10^{-4})$	$-4.66 \times 10^{-3}(1.08 \times 10^{-4})$	$-1.14 \times 10^{-2}(1.23 \times 10^{-4})$	$-5.76 \times 10^{-3}(9.45 \times 10^{-5})$
$\mathbf{Z_w}$	$1.52 \times 10^{-3}(6.89 \times 10^{-4})$	$2.44 \times 10^{-3}(3.44 \times 10^{-4})$	$-2.73 \times 10^{-2}(4.42 \times 10^{-4})$	$-1.40 \times 10^{-2}(4.25 \times 10^{-4})$

Param.	Model # 9	10	11	12
$\mathbf{M_q}$	$-6.29 \times 10^{-4}(3.25 \times 10^{-5})$	$-3.08 \times 10^{-4}(2.26 \times 10^{-6})$	$-5.12 \times 10^{-4}(3.83 \times 10^{-6})$	$-4.90 \times 10^{-4}(3.15 \times 10^{-6})$
$\mathbf{M_u}$	$-1.11 \times 10^{-3}(1.70 \times 10^{-4})$	$-1.69 \times 10^{-3}(1.53 \times 10^{-5})$	$-1.03 \times 10^{-3}(2.53 \times 10^{-5})$	$-1.31 \times 10^{-3}(1.47 \times 10^{-5})$
$\mathbf{M_w}$	$-6.58 \times 10^{-3}(1.94 \times 10^{-4})$	$-4.98 \times 10^{-4}(2.41 \times 10^{-5})$	$-2.41 \times 10^{-3}(4.08 \times 10^{-5})$	$-1.58 \times 10^{-3}(1.97 \times 10^{-5})$
$\mathbf{M_{\delta_e}}$	$1.60 \times 10^{-3}(7.54 \times 10^{-5})$	$1.16 \times 10^{-3}(9.48 \times 10^{-6})$	$1.66 \times 10^{-3}(1.37 \times 10^{-5})$	$1.81 \times 10^{-3}(1.30 \times 10^{-5})$
$\mathbf{X_q}$	$6.38 \times 10^{-3}(6.36 \times 10^{-4})$	$1.66 \times 10^{-2}(1.49 \times 10^{-4})$	$1.92 \times 10^{-2}(1.20 \times 10^{-4})$	$1.58 \times 10^{-2}(1.20 \times 10^{-4})$
$\mathbf{X_u}$	$-9.56 \times 10^{-2}(2.03 \times 10^{-3})$	$-1.53 \times 10^{-1}(6.17 \times 10^{-4})$	$-1.51 \times 10^{-1}(4.77 \times 10^{-4})$	$-1.40 \times 10^{-1}(4.94 \times 10^{-4})$
$\mathbf{X_{\delta_e}}$	$-2.89 \times 10^{-2}(1.97 \times 10^{-3})$	$-2.27 \times 10^{-2}(5.82 \times 10^{-4})$	$-3.46 \times 10^{-2}(5.37 \times 10^{-4})$	$-2.51 \times 10^{-2}(6.27 \times 10^{-4})$
$\mathbf{Z_q}$	$-1.83 \times 10^{-2}(1.32 \times 10^{-3})$	$-3.19 \times 10^{-3}(3.05 \times 10^{-4})$	$-2.88 \times 10^{-3}(2.09 \times 10^{-4})$	$3.71 \times 10^{-4}(2.11 \times 10^{-4})$
$\mathbf{Z_w}$	$-7.63 \times 10^{-2}(3.17 \times 10^{-3})$	$-2.33 \times 10^{-2}(1.08 \times 10^{-3})$	$-7.81 \times 10^{-3}(1.00 \times 10^{-3})$	$1.41 \times 10^{-2}(6.48 \times 10^{-4})$

Param.	Model # 13	14	15	16
$\mathbf{M_q}$	$-5.36 \times 10^{-4}(2.75 \times 10^{-6})$	$-6.10 \times 10^{-4}(2.79 \times 10^{-6})$	$-7.96 \times 10^{-4}(5.43 \times 10^{-6})$	$-5.88 \times 10^{-4}(1.06 \times 10^{-5})$
$\mathbf{M_u}$	$-2.03 \times 10^{-3}(1.22 \times 10^{-5})$	$-2.22 \times 10^{-3}(1.54 \times 10^{-5})$	$-1.11 \times 10^{-3}(1.92 \times 10^{-5})$	$-1.85 \times 10^{-3}(5.17 \times 10^{-5})$
$\mathbf{M_w}$	$-8.08 \times 10^{-4}(1.69 \times 10^{-5})$	$-1.54 \times 10^{-3}(2.01 \times 10^{-5})$	$-2.77 \times 10^{-3}(2.80 \times 10^{-5})$	$-2.75 \times 10^{-3}(1.02 \times 10^{-4})$
$\mathbf{M_{\delta_e}}$	$2.13 \times 10^{-3}(1.38 \times 10^{-5})$	$2.06 \times 10^{-3}(1.40 \times 10^{-5})$	$2.51 \times 10^{-3}(2.01 \times 10^{-5})$	$1.57 \times 10^{-3}(1.93 \times 10^{-5})$
$\mathbf{X_q}$	$1.83 \times 10^{-2}(9.88 \times 10^{-5})$	$2.51 \times 10^{-2}(2.30 \times 10^{-4})$	$2.52 \times 10^{-2}(3.55 \times 10^{-4})$	$2.13 \times 10^{-2}(1.34 \times 10^{-4})$
$\mathbf{X_u}$	$-1.47 \times 10^{-1}(4.44 \times 10^{-4})$	$-1.36 \times 10^{-1}(1.00 \times 10^{-3})$	$-1.33 \times 10^{-1}(1.45 \times 10^{-3})$	$-1.51 \times 10^{-1}(6.02 \times 10^{-4})$
$\mathbf{X_{\delta_e}}$	$-4.09 \times 10^{-2}(4.53 \times 10^{-4})$	$-6.99 \times 10^{-2}(1.08 \times 10^{-3})$	$-7.31 \times 10^{-2}(1.61 \times 10^{-3})$	$-3.88 \times 10^{-2}(4.90 \times 10^{-4})$
$\mathbf{Z_q}$	$5.17 \times 10^{-4}(2.30 \times 10^{-4})$	$-1.96 \times 10^{-3}(8.62 \times 10^{-5})$	$-3.61 \times 10^{-3}(1.21 \times 10^{-4})$	$-1.64 \times 10^{-2}(5.88 \times 10^{-4})$
$\mathbf{Z_w}$	$4.41 \times 10^{-3}(8.45 \times 10^{-4})$	$1.22 \times 10^{-2}(4.72 \times 10^{-4})$	$-5.91 \times 10^{-3}(5.02 \times 10^{-4})$	$-9.14 \times 10^{-2}(3.32 \times 10^{-3})$

Param.	Model # 17	18	19	20
$\mathbf{M_q}$	$-4.94 \times 10^{-4}(3.00 \times 10^{-6})$	$-4.95 \times 10^{-4}(3.61 \times 10^{-6})$	$-7.24 \times 10^{-4}(5.31 \times 10^{-6})$	$-6.12 \times 10^{-4}(4.52 \times 10^{-6})$
$\mathbf{M_u}$	$-1.48 \times 10^{-3}(9.26 \times 10^{-6})$	$-1.43 \times 10^{-3}(1.82 \times 10^{-5})$	$-1.63 \times 10^{-3}(3.61 \times 10^{-5})$	$-1.90 \times 10^{-3}(2.38 \times 10^{-5})$
$\mathbf{M_w}$	$-7.73 \times 10^{-4}(9.74 \times 10^{-6})$	$-1.64 \times 10^{-3}(2.05 \times 10^{-5})$	$-1.58 \times 10^{-3}(3.77 \times 10^{-5})$	$-1.41 \times 10^{-3}(1.68 \times 10^{-5})$
$\mathbf{M_{\delta_e}}$	$1.75 \times 10^{-3}(1.38 \times 10^{-5})$	$2.11 \times 10^{-3}(1.68 \times 10^{-5})$	$2.43 \times 10^{-3}(1.65 \times 10^{-5})$	$2.17 \times 10^{-3}(1.66 \times 10^{-5})$
$\mathbf{X_q}$	$2.08 \times 10^{-2}(1.45 \times 10^{-4})$	$2.08 \times 10^{-2}(1.14 \times 10^{-4})$	$1.89 \times 10^{-2}(2.98 \times 10^{-4})$	$2.38 \times 10^{-2}(2.30 \times 10^{-4})$
$\mathbf{X_u}$	$-1.62 \times 10^{-1}(6.29 \times 10^{-4})$	$-1.61 \times 10^{-1}(5.64 \times 10^{-4})$	$-1.60 \times 10^{-1}(1.12 \times 10^{-3})$	$-1.80 \times 10^{-1}(1.00 \times 10^{-3})$
$\mathbf{X_{\delta_e}}$	$-5.01 \times 10^{-2}(6.24 \times 10^{-4})$	$-4.09 \times 10^{-2}(5.86 \times 10^{-4})$	$-1.94 \times 10^{-2}(1.23 \times 10^{-3})$	$-4.99 \times 10^{-2}(7.12 \times 10^{-4})$
$\mathbf{Z_q}$	$9.00 \times 10^{-4}(1.36 \times 10^{-4})$	$-9.19 \times 10^{-4}(1.97 \times 10^{-4})$	$-6.76 \times 10^{-3}(3.04 \times 10^{-4})$	$-2.31 \times 10^{-3}(1.80 \times 10^{-4})$
$\mathbf{Z_w}$	$2.15 \times 10^{-2}(4.60 \times 10^{-4})$	$-5.21 \times 10^{-3}(6.70 \times 10^{-4})$	$-2.72 \times 10^{-2}(8.39 \times 10^{-4})$	$-1.41 \times 10^{-2}(3.53 \times 10^{-4})$

Param.	Model # 21	22	23	24
$\mathbf{M_q}$	$-5.55 \times 10^{-4}(6.26 \times 10^{-6})$	$-7.44 \times 10^{-4}(3.31 \times 10^{-6})$	$-5.09 \times 10^{-4}(5.31 \times 10^{-6})$	$-8.52 \times 10^{-4}(5.53 \times 10^{-6})$
$\mathbf{M_u}$	$-1.87 \times 10^{-3}(3.37 \times 10^{-5})$	$-1.40 \times 10^{-3}(1.15 \times 10^{-5})$	$-2.63 \times 10^{-3}(2.39 \times 10^{-5})$	$-6.71 \times 10^{-4}(2.55 \times 10^{-5})$
$\mathbf{M_w}$	$-1.27 \times 10^{-3}(2.27 \times 10^{-5})$	$-1.49 \times 10^{-3}(9.91 \times 10^{-6})$	$9.76 \times 10^{-5}(1.19 \times 10^{-5})$	$-2.60 \times 10^{-3}(2.51 \times 10^{-5})$
$\mathbf{M_{\delta_e}}$	$1.27 \times 10^{-3}(1.76 \times 10^{-5})$	$2.78 \times 10^{-3}(1.38 \times 10^{-5})$	$2.54 \times 10^{-3}(2.00 \times 10^{-5})$	$2.82 \times 10^{-3}(1.62 \times 10^{-5})$
$\mathbf{X_q}$	$2.98 \times 10^{-2}(2.51 \times 10^{-4})$	$2.00 \times 10^{-2}(1.79 \times 10^{-4})$	$9.98 \times 10^{-3}(3.03 \times 10^{-4})$	$2.93 \times 10^{-2}(2.00 \times 10^{-4})$
$\mathbf{X_u}$	$-1.92 \times 10^{-1}(1.36 \times 10^{-3})$	$-1.69 \times 10^{-1}(8.51 \times 10^{-4})$	$-1.65 \times 10^{-1}(1.73 \times 10^{-3})$	$-1.60 \times 10^{-1}(8.24 \times 10^{-4})$
$\mathbf{X_{\delta_e}}$	$-5.69 \times 10^{-2}(7.41 \times 10^{-4})$	$-4.24 \times 10^{-2}(6.20 \times 10^{-4})$	$6.49 \times 10^{-2}(1.02 \times 10^{-3})$	$-6.33 \times 10^{-2}(8.17 \times 10^{-4})$
$\mathbf{Z_q}$	$-2.58 \times 10^{-3}(2.68 \times 10^{-4})$	$-3.56 \times 10^{-3}(1.06 \times 10^{-4})$	$3.14 \times 10^{-3}(1.25 \times 10^{-4})$	$-8.00 \times 10^{-3}(1.74 \times 10^{-4})$
$\mathbf{Z_w}$	$-2.74 \times 10^{-2}(7.57 \times 10^{-4})$	$-2.29 \times 10^{-2}(4.13 \times 10^{-4})$	$1.23 \times 10^{-2}(4.60 \times 10^{-4})$	$-3.74 \times 10^{-2}(4.00 \times 10^{-4})$

Param.	Model # 25	26	27	28
$\mathbf{M_q}$	$-5.87 \times 10^{-4}(3.91 \times 10^{-6})$	$-7.12 \times 10^{-4}(4.32 \times 10^{-6})$	$-7.75 \times 10^{-4}(3.21 \times 10^{-6})$	$-7.77 \times 10^{-4}(6.19 \times 10^{-6})$
$\mathbf{M_u}$	$-1.34 \times 10^{-3}(2.00 \times 10^{-5})$	$-1.81 \times 10^{-3}(1.50 \times 10^{-5})$	$-8.26 \times 10^{-4}(1.62 \times 10^{-5})$	$-1.20 \times 10^{-3}(4.54 \times 10^{-5})$
$\mathbf{M_w}$	$-1.25 \times 10^{-3}(1.67 \times 10^{-5})$	$-1.30 \times 10^{-3}(1.44 \times 10^{-5})$	$-1.93 \times 10^{-3}(1.26 \times 10^{-5})$	$-2.28 \times 10^{-3}(3.11 \times 10^{-5})$
$\mathbf{M_{\delta_e}}$	$2.32 \times 10^{-3}(1.65 \times 10^{-5})$	$2.30 \times 10^{-3}(1.51 \times 10^{-5})$	$2.72 \times 10^{-3}(1.15 \times 10^{-5})$	$2.78 \times 10^{-3}(2.06 \times 10^{-5})$

$\mathbf{X_q}$	$2.25 \times 10^{-2}(3.19 \times 10^{-4})$	$2.59 \times 10^{-2}(1.49 \times 10^{-4})$	$2.29 \times 10^{-2}(2.04 \times 10^{-4})$	$2.45 \times 10^{-2}(4.76 \times 10^{-4})$
$\mathbf{X_u}$	$-1.74 \times 10^{-1}(1.49 \times 10^{-3})$	$-1.73 \times 10^{-1}(6.89 \times 10^{-4})$	$-1.90 \times 10^{-1}(9.48 \times 10^{-4})$	$-2.17 \times 10^{-1}(2.58 \times 10^{-3})$
$\mathbf{X_{\delta_e}}$	$-4.35 \times 10^{-2}(1.67 \times 10^{-3})$	$-5.19 \times 10^{-2}(6.11 \times 10^{-4})$	$-5.57 \times 10^{-2}(9.12 \times 10^{-4})$	$-4.40 \times 10^{-2}(1.51 \times 10^{-3})$
$\mathbf{Z_q}$	$-4.43 \times 10^{-3}(1.54 \times 10^{-4})$	$-5.25 \times 10^{-3}(1.10 \times 10^{-4})$	$-1.89 \times 10^{-3}(1.12 \times 10^{-4})$	$-7.68 \times 10^{-3}(1.86 \times 10^{-4})$
$\mathbf{Z_w}$	$-1.96 \times 10^{-2}(5.51 \times 10^{-4})$	$-2.39 \times 10^{-2}(3.98 \times 10^{-4})$	$-1.57 \times 10^{-2}(2.92 \times 10^{-4})$	$-3.58 \times 10^{-2}(5.41 \times 10^{-4})$

Param.	Model # 29	30	31	32
$\mathbf{M_q}$	$-8.14 \times 10^{-4}(5.41 \times 10^{-6})$	$-5.80 \times 10^{-4}(2.49 \times 10^{-6})$	$-7.96 \times 10^{-4}(3.74 \times 10^{-6})$	$-4.94 \times 10^{-4}(2.63 \times 10^{-6})$
$\mathbf{M_u}$	$-1.21 \times 10^{-3}(1.39 \times 10^{-5})$	$-2.19 \times 10^{-3}(8.94 \times 10^{-6})$	$-2.83 \times 10^{-4}(1.74 \times 10^{-5})$	$-1.14 \times 10^{-3}(1.22 \times 10^{-5})$
$\mathbf{M_w}$	$-1.72 \times 10^{-3}(1.44 \times 10^{-5})$	$-5.13 \times 10^{-4}(5.21 \times 10^{-6})$	$-2.02 \times 10^{-3}(1.34 \times 10^{-5})$	$-9.03 \times 10^{-4}(9.02 \times 10^{-6})$
$\mathbf{M_{\delta_e}}$	$3.07 \times 10^{-3}(2.15 \times 10^{-5})$	$2.29 \times 10^{-3}(9.28 \times 10^{-6})$	$2.70 \times 10^{-3}(1.34 \times 10^{-5})$	$2.03 \times 10^{-3}(1.28 \times 10^{-5})$
$\mathbf{X_q}$	$2.81 \times 10^{-2}(2.27 \times 10^{-4})$	$2.10 \times 10^{-2}(1.65 \times 10^{-4})$	$1.98 \times 10^{-2}(4.30 \times 10^{-4})$	$2.44 \times 10^{-2}(1.72 \times 10^{-4})$
$\mathbf{X_u}$	$-1.67 \times 10^{-1}(1.09 \times 10^{-3})$	$-1.84 \times 10^{-1}(9.56 \times 10^{-4})$	$-1.62 \times 10^{-1}(1.82 \times 10^{-3})$	$-1.95 \times 10^{-1}(8.51 \times 10^{-4})$
$\mathbf{X_{\delta_e}}$	$-5.73 \times 10^{-2}(8.77 \times 10^{-4})$	$-4.55 \times 10^{-2}(4.00 \times 10^{-4})$	$-4.89 \times 10^{-2}(1.15 \times 10^{-3})$	$-4.85 \times 10^{-2}(8.56 \times 10^{-4})$
$\mathbf{Z_q}$	$-3.87 \times 10^{-3}(1.42 \times 10^{-4})$	$-3.19 \times 10^{-3}(7.68 \times 10^{-5})$	$-4.80 \times 10^{-4}(1.38 \times 10^{-4})$	$-1.65 \times 10^{-4}(1.41 \times 10^{-4})$
$\mathbf{Z_w}$	$-2.20 \times 10^{-2}(3.19 \times 10^{-4})$	$-1.55 \times 10^{-2}(2.98 \times 10^{-4})$	$-1.90 \times 10^{-2}(3.22 \times 10^{-4})$	$-1.30 \times 10^{-2}(4.70 \times 10^{-4})$

Param.	Model # 33	34	35	36
$\mathbf{M_q}$	$-6.82 \times 10^{-4}(2.41 \times 10^{-6})$	$-5.43 \times 10^{-4}(2.80 \times 10^{-6})$	$-6.35 \times 10^{-4}(3.49 \times 10^{-6})$	$-7.61 \times 10^{-4}(5.16 \times 10^{-6})$
$\mathbf{M_u}$	$-1.17 \times 10^{-3}(9.55 \times 10^{-6})$	$-8.18 \times 10^{-4}(1.89 \times 10^{-5})$	$-1.56 \times 10^{-3}(1.51 \times 10^{-5})$	$-3.54 \times 10^{-4}(2.95 \times 10^{-5})$
$\mathbf{M_w}$	$-1.21 \times 10^{-3}(7.38 \times 10^{-6})$	$-9.63 \times 10^{-4}(8.24 \times 10^{-6})$	$-7.86 \times 10^{-4}(8.60 \times 10^{-6})$	$-2.27 \times 10^{-3}(2.54 \times 10^{-5})$
$\mathbf{M_{\delta_e}}$	$2.58 \times 10^{-3}(1.01 \times 10^{-5})$	$2.09 \times 10^{-3}(1.39 \times 10^{-5})$	$2.84 \times 10^{-3}(1.43 \times 10^{-5})$	$2.65 \times 10^{-3}(1.92 \times 10^{-5})$
$\mathbf{X_q}$	$2.11 \times 10^{-2}(1.82 \times 10^{-4})$	$2.94 \times 10^{-2}(2.22 \times 10^{-4})$	$3.68 \times 10^{-2}(2.00 \times 10^{-4})$	$2.99 \times 10^{-2}(2.69 \times 10^{-4})$
$\mathbf{X_u}$	$-1.82 \times 10^{-1}(8.21 \times 10^{-4})$	$-2.30 \times 10^{-1}(1.44 \times 10^{-3})$	$-2.14 \times 10^{-1}(1.03 \times 10^{-3})$	$-1.49 \times 10^{-1}(1.14 \times 10^{-3})$
$\mathbf{X_{\delta_e}}$	$-3.56 \times 10^{-2}(5.62 \times 10^{-4})$	$-8.15 \times 10^{-2}(7.64 \times 10^{-4})$	$-1.02 \times 10^{-1}(9.06 \times 10^{-4})$	$-7.00 \times 10^{-2}(1.27 \times 10^{-3})$
$\mathbf{Z_q}$	$-2.28 \times 10^{-3}(9.14 \times 10^{-5})$	$-5.89 \times 10^{-4}(2.48 \times 10^{-4})$	$-5.07 \times 10^{-3}(1.28 \times 10^{-4})$	$-4.58 \times 10^{-3}(2.25 \times 10^{-4})$
$\mathbf{Z_w}$	$-1.94 \times 10^{-2}(2.81 \times 10^{-4})$	$-1.01 \times 10^{-2}(4.60 \times 10^{-4})$	$-2.86 \times 10^{-2}(3.58 \times 10^{-4})$	$-2.73 \times 10^{-2}(6.46 \times 10^{-4})$

Param.	Model # 37	38	39	40
$\mathbf{M_q}$	$-9.07 \times 10^{-4}(6.73 \times 10^{-6})$	$-7.74 \times 10^{-4}(5.00 \times 10^{-6})$	$-6.31 \times 10^{-4}(3.68 \times 10^{-6})$	$-6.23 \times 10^{-4}(4.23 \times 10^{-6})$
$\mathbf{M_u}$	$-4.02 \times 10^{-4}(3.98 \times 10^{-5})$	$-3.63 \times 10^{-4}(2.01 \times 10^{-5})$	$-1.78 \times 10^{-3}(2.44 \times 10^{-5})$	$-1.07 \times 10^{-3}(2.21 \times 10^{-5})$
$\mathbf{M_w}$	$-1.94 \times 10^{-3}(1.96 \times 10^{-5})$	$-1.39 \times 10^{-3}(1.18 \times 10^{-5})$	$-7.34 \times 10^{-4}(6.96 \times 10^{-6})$	$-1.25 \times 10^{-3}(1.27 \times 10^{-5})$
$\mathbf{M_{\delta_e}}$	$3.15 \times 10^{-3}(1.63 \times 10^{-5})$	$2.73 \times 10^{-3}(1.80 \times 10^{-5})$	$2.28 \times 10^{-3}(1.55 \times 10^{-5})$	$2.22 \times 10^{-3}(1.47 \times 10^{-5})$
$\mathbf{X_q}$	$2.66 \times 10^{-2}(3.28 \times 10^{-4})$	$3.33 \times 10^{-2}(4.12 \times 10^{-4})$	$3.99 \times 10^{-2}(2.81 \times 10^{-4})$	$3.01 \times 10^{-2}(1.59 \times 10^{-4})$
$\mathbf{X_u}$	$-1.83 \times 10^{-1}(1.21 \times 10^{-3})$	$-2.10 \times 10^{-1}(1.99 \times 10^{-3})$	$-2.71 \times 10^{-1}(1.76 \times 10^{-3})$	$-2.43 \times 10^{-1}(9.73 \times 10^{-4})$
$\mathbf{X_{\delta_e}}$	$-3.80 \times 10^{-2}(8.74 \times 10^{-4})$	$-7.02 \times 10^{-2}(1.80 \times 10^{-3})$	$-1.04 \times 10^{-1}(1.02 \times 10^{-3})$	$-7.69 \times 10^{-2}(6.79 \times 10^{-4})$
$\mathbf{Z_q}$	$-1.06 \times 10^{-2}(3.90 \times 10^{-4})$	$1.24 \times 10^{-3}(2.15 \times 10^{-4})$	$1.39 \times 10^{-3}(2.78 \times 10^{-4})$	$-7.85 \times 10^{-3}(2.27 \times 10^{-4})$
$\mathbf{Z_w}$	$-4.13 \times 10^{-2}(4.40 \times 10^{-4})$	$-1.46 \times 10^{-2}(3.21 \times 10^{-4})$	$-2.08 \times 10^{-2}(3.78 \times 10^{-4})$	$-3.17 \times 10^{-2}(3.58 \times 10^{-4})$

Param.	Model # 41	42	43	44
$\mathbf{M_q}$	$-4.97 \times 10^{-4}(3.56 \times 10^{-6})$	$-7.77 \times 10^{-4}(3.92 \times 10^{-6})$	$-6.98 \times 10^{-4}(4.29 \times 10^{-6})$	$-7.46 \times 10^{-4}(6.06 \times 10^{-6})$
$\mathbf{M_u}$	$-1.09 \times 10^{-3}(2.61 \times 10^{-5})$	$-5.43 \times 10^{-4}(1.82 \times 10^{-5})$	$-6.29 \times 10^{-4}(1.82 \times 10^{-5})$	$-9.33 \times 10^{-5}(3.38 \times 10^{-5})$
$\mathbf{M_w}$	$-7.71 \times 10^{-4}(1.33 \times 10^{-5})$	$-1.21 \times 10^{-3}(8.84 \times 10^{-6})$	$-1.44 \times 10^{-3}(1.38 \times 10^{-5})$	$-1.40 \times 10^{-3}(2.06 \times 10^{-5})$
$\mathbf{M_{\delta_e}}$	$2.17 \times 10^{-3}(1.72 \times 10^{-5})$	$3.09 \times 10^{-3}(1.51 \times 10^{-5})$	$2.83 \times 10^{-3}(1.78 \times 10^{-5})$	$3.07 \times 10^{-3}(2.38 \times 10^{-5})$
$\mathbf{X_q}$	$2.73 \times 10^{-2}(1.40 \times 10^{-4})$	$3.27 \times 10^{-2}(1.53 \times 10^{-4})$	$2.82 \times 10^{-2}(3.27 \times 10^{-4})$	$3.27 \times 10^{-2}(2.12 \times 10^{-4})$
$\mathbf{X_u}$	$-2.21 \times 10^{-1}(7.73 \times 10^{-4})$	$-2.30 \times 10^{-1}(7.34 \times 10^{-4})$	$-1.70 \times 10^{-1}(1.51 \times 10^{-3})$	$-1.98 \times 10^{-1}(9.04 \times 10^{-4})$
$\mathbf{X_{\delta_e}}$	$-6.63 \times 10^{-2}(6.78 \times 10^{-4})$	$-6.96 \times 10^{-2}(7.08 \times 10^{-4})$	$-5.35 \times 10^{-2}(9.03 \times 10^{-4})$	$-6.48 \times 10^{-2}(9.02 \times 10^{-4})$
$\mathbf{Z_q}$	$-9.46 \times 10^{-4}(3.67 \times 10^{-4})$	$-1.33 \times 10^{-3}(1.76 \times 10^{-4})$	$-9.55 \times 10^{-3}(2.01 \times 10^{-4})$	$-7.60 \times 10^{-3}(3.54 \times 10^{-4})$
$\mathbf{Z_w}$	$-1.58 \times 10^{-2}(8.34 \times 10^{-4})$	$-2.02 \times 10^{-2}(2.36 \times 10^{-4})$	$-3.18 \times 10^{-2}(3.92 \times 10^{-4})$	$-3.44 \times 10^{-2}(6.95 \times 10^{-4})$

Param.	Model # 45	46
$\mathbf{M_q}$	$-6.25 \times 10^{-4}(3.64 \times 10^{-6})$	$-6.70 \times 10^{-4}(3.04 \times 10^{-6})$
$\mathbf{M_u}$	$-1.67 \times 10^{-3}(3.04 \times 10^{-5})$	$-2.22 \times 10^{-3}(1.71 \times 10^{-5})$
$\mathbf{M_w}$	$-5.70 \times 10^{-4}(6.73 \times 10^{-6})$	$-5.81 \times 10^{-4}(8.09 \times 10^{-6})$
$\mathbf{M_{\delta_e}}$	$2.50 \times 10^{-3}(1.94 \times 10^{-5})$	$2.76 \times 10^{-3}(1.18 \times 10^{-5})$
$\mathbf{X_q}$	$3.42 \times 10^{-2}(3.00 \times 10^{-4})$	$2.49 \times 10^{-2}(2.90 \times 10^{-4})$
$\mathbf{X_u}$	$-2.75 \times 10^{-1}(2.20 \times 10^{-3})$	$-2.19 \times 10^{-1}(1.89 \times 10^{-3})$
$\mathbf{X_{\delta_e}}$	$-1.10 \times 10^{-1}(1.40 \times 10^{-3})$	$-5.26 \times 10^{-2}(1.22 \times 10^{-3})$
$\mathbf{Z_q}$	$3.31 \times 10^{-4}(3.49 \times 10^{-4})$	$-6.06 \times 10^{-3}(1.00 \times 10^{-4})$
$\mathbf{Z_w}$	$-1.89 \times 10^{-2}(5.74 \times 10^{-4})$	$-2.99 \times 10^{-2}(2.50 \times 10^{-4})$